This paper appears in IEEE Transactions on Cybernetics, 2021.
Digital Object Identifier: 10.1109/TCYB.2020.3043798

Impedance Variation and Learning Strategies in Human-Robot Interaction

Mojtaba Sharifi[a,b,c], Amir Zakerimanesh[a,c], Javad K. Mehr[a,b,c], Ali Torabi[a,c], Vivian K. Mushahwar[b,c], Mahdi Tavakoli[a,c]

***Abstract*—In this survey, various concepts and methodologies developed over the past two decades for varying and learning the impedance or admittance of robotic systems that physically interact with humans are explored. For this purpose, the assumptions and mathematical formulations for online adjustment of impedance models and controllers for physical human-robot interaction (HRI) are categorized and compared. In this systematic review, studies on (a) variation and (b) learning of appropriate impedance elements are taken into account. These strategies are classified and described in terms of their objectives, points of view (approaches), signal requirements (including position, HRI force and EMG activity). Different methods involving linear/nonlinear analyses (e.g., optimal control design and nonlinear Lyapunov-based stability guarantee) and Gaussian approximation algorithms (e.g., GMM-based and DMP-based strategies) are reviewed. Current challenges and research trends in physical HRI are finally discussed.**

***Index Terms*—Human-robot interaction (HRI); impedance and admittance models; impedance variation; impedance learning; impedance control; robot learning; robot stability.**

I. Introduction

Impedance and its reciprocal, admittance, play an essential role in physical human-robot interaction (HRI) by defining a mathematical relationship between force and position. The objective of the controller of a robotic system can be amended from pure position or force control to impedance and/or admittance control in order to perform more physically challenging tasks [1]. Accordingly, robot impedance adjustment has been the center of many research studies over the past three decades in the fields of robotics and HRI [2], [3]. Considerable progress has been made through the development of sophisticated control strategies involving the dynamics and kinematics of multi-DOF robots [4]. Although most of these studies focused on impedance/admittance models with constant parameters, others have focused on state-dependent, time-varying impedance control and online learning of impedance parameters in different applications of HRI.

Impedance variation and learning for robotic systems have been inspired by human behavior. The human limb's impedance is continuously modified by the central nervous system (CNS) based on the task requirements [5], [6], [7], [8], and the same strategy can be mimicked by robots during HRI [9], [10]. Depending on each collaborative task objective and human physical behavior, the robot impedance parameters can be modulated and changed in real-time autonomously [11]. For instance, it was shown that the tasks of inserting a peg into a tight hole and throwing a switch without overshooting cannot be optimally facilitated by the same impedance level for the robot [12]. Walker *et al.* [12] showed that amending the robot impedance in harmony with the operator's hand impedance could improve the performance of these two tasks. Variable impedance provides versatility for the robot that can change its dynamics according to the task requirements and human physical behavior. However, this requires adequate knowledge and modeling of the robot, task and human limb.

In recent years, several impedance adaptation strategies have been proposed and tested in the robot's joint and Cartesian spaces, which are explained in the present review paper. In Section II, the nonlinear dynamic structure of multi-DOF robots and typical desired impedance/admittance models in the joint and task coordinates are presented. The main methods underlying online impedance variation are discussed in Section III, and are categorized based on velocity, force and EMG signals in addition to stability criteria. In Section IV, various learning algorithms for online adjustment of impedance parameters are described and classified based on their analyses, including optimization and learning from demonstration using position, force and EMG data. Finally, current research trends and future challenges of online impedance adaptation in HRI applications are discussed in Section V.

II. Desired Impedance Models

The joint-space dynamics of a robot with n joints and m Cartesian coordinates can be represented as

$$\mathbf{M}_q\ddot{\mathbf{q}} + \mathbf{C}_q\dot{\mathbf{q}} + \mathbf{g}_q + \boldsymbol{\tau}_{frc} = \boldsymbol{\tau}_c + \boldsymbol{\tau}_e \tag{1}$$

where $\mathbf{q} \in \mathbb{R}^{n\times 1}$ is the vector of joint positions, $\mathbf{M}_q \in \mathbb{R}^{n\times n}$ is the inertia matrix, $\mathbf{C}_q \in \mathbb{R}^{n\times n}$ is the matrix of Coriolis and centrifugal terms, $\mathbf{g}_q \in \mathbb{R}^{n\times 1}$ is the vector of gravitational torques, $\boldsymbol{\tau}_{frc} \in \mathbb{R}^{n\times 1}$ is the vector of the friction torques, $\boldsymbol{\tau}_c \in \mathbb{R}^{n\times 1}$ is the control torque, and $\boldsymbol{\tau}_e = \mathbf{J}^T\mathbf{f}_e$ is the external torque in which $\mathbf{f}_e \in \mathbb{R}^{m\times 1}$ is the external force applied on the end-effector of the robot and $\mathbf{J} \in \mathbb{R}^{m\times n}$ is the robot Jacobian matrix. The end-effector dynamics of a robot in the Cartesian space can be written as [13]

$$\mathbf{M}_x\ddot{\mathbf{x}} + \mathbf{C}_x\dot{\mathbf{x}} + \mathbf{g}_x + \mathbf{f}_{frc} = \mathbf{f}_c + \mathbf{f}_e \tag{2}$$

Manuscript received August 24, 2020 (Corresponding author: Mojtaba Sharifi)

[a]Department of Electrical and Computer Engineering, University of Alberta, Edmonton, Alberta, Canada T6G 1H9 (e-mail: M.Sharifi@ualberta.ca; Amir.Zakerimanesh@ualberta.ca; J.Khodaeimehr@ualberta.ca; Ali.Torabi@ualberta.ca; Mahdi.Tavakoli@ualberta.ca)

[b]Department of Medicine, Division of Physical Medicine and Rehabilitation, University of Alberta, Edmonton, Alberta, Canada T6G 2E1 (e-mail: M.Sharifi@ualberta.ca; Vivian.Mushahwar@ualberta.ca)

[c]Sensory Motor Adaptive Rehabilitation Technology (SMART) Network, University of Alberta, Edmonton, Alberta, Canada T6G 2E1

in which $\mathbf{x} \in \mathbb{R}^{m\times 1}$ is the vector of end-effector position/orientation (pose), $\mathbf{M}_x = \left(\mathbf{J}\mathbf{M}_q^{-1}\mathbf{J}^T\right)^{-1} \in \mathbb{R}^{m\times m}$ is the end-effector inertia matrix, $\mathbf{C}_x = \mathbf{M}_x\left(\mathbf{J}\mathbf{M}_q^{-1}\mathbf{C}_q - \dot{\mathbf{J}}\right)\mathbf{J}^\dagger \in \mathbb{R}^{m\times m}$ is the matrix of the end-effector's centrifugal and Coriolis terms, $\mathbf{g}_x = \mathbf{J}^{\dagger T}\mathbf{g}_q \in \mathbb{R}^{m\times 1}$ is the vector of gravitational wrench and $\mathbf{f}_{frc} = \mathbf{J}^{\dagger T}\boldsymbol{\tau}_{frc} \in \mathbb{R}^{m\times 1}$ is the vector of friction wrench reflected at the end-effector, and $\mathbf{f}_c = \mathbf{J}^{\dagger T}\boldsymbol{\tau}_c \in \mathbb{R}^{m\times 1}$ is the Cartesian-space control wrench. Moreover, $\mathbf{J}^\dagger$ is generalized inverse of the Jacobian matrix defined in [13] as

$$\mathbf{J}^\dagger = \mathbf{M}_q^{-1}\mathbf{J}^T\left[\mathbf{J}\mathbf{M}_q^{-1}\mathbf{J}^T\right]^{-1}. \tag{3}$$

Note that replacing $\mathbf{M}_q$ with the identity matrix $\mathbb{I}_{n\times n}$ will change this generalized form to the right pseudoinverse.

The desired Cartesian-space impedance model of the robot is considered as

$$\mathbf{M}_x^d\ddot{\tilde{\mathbf{x}}}_d + \mathbf{B}_x^d\dot{\tilde{\mathbf{x}}}_d + \mathbf{K}_x^d\tilde{\mathbf{x}}_d = \mathbf{f}_e \tag{4}$$

where $\mathbf{M}_x^d$, $\mathbf{B}_x^d$, and $\mathbf{K}_x^d$ are the desired Cartesian inertia, damping, and stiffness matrices, respectively, and $\tilde{\mathbf{x}}_d = \mathbf{x}_d - \mathbf{x}_0 \in \mathbb{R}^{m\times 1}$ is the deviation of the desired end-effector position from $\mathbf{x}_0$ that is initially designed to be tracked in the absence of the interaction force $\mathbf{f}_e$. Also, the desired joint-space impedance model is defined as

$$\mathbf{M}_q^d\ddot{\tilde{\mathbf{q}}}_d + \mathbf{B}_q^d\dot{\tilde{\mathbf{q}}}_d + \mathbf{K}_q^d\tilde{\mathbf{q}}_d = \boldsymbol{\tau}_e \tag{5}$$

where $\tilde{\mathbf{q}}_d = \mathbf{q}_d - \mathbf{q}_0$ is the desired joint trajectory deviation with respect to $\mathbf{q}_0$ as the initial HRI-free trajectory. $\mathbf{M}_q^d \in \mathbb{R}^{n\times n}$, $\mathbf{B}_q^d \in \mathbb{R}^{n\times n}$ and $\mathbf{K}_q^d \in \mathbb{R}^{n\times n}$ denote the desired joint inertia, damping and stiffness values, respectively.

Different strategies on online regulation and learning of the robot impedance in physical HRI are explained in the next two sections. Significant objectives, requirements and characteristics of these methods are summarized in Table I. Velocity, force and stability control of robotic systems have been taken into consideration as the primary purposes. The position and force feedback from the robot and the EMG data from the human muscles are required in these schemes. Other aspects of these studies are also outlined in Table I in terms of their benefits and drawbacks.

III. Impedance Variation Methods

The objective of variable impedance control (VIC) is to modulate the desired stiffness, damping and inertia of the robot in order to improve the robot's compliance and/or stability during its interaction with the human. One of the main purposes of impedance regulation in HRIs is to maintain a force range between the robot and user [14] based on task specifications (e.g., velocity magnitude or positioning accuracy).

A. Velocity-Based Approaches

In physical HRI, the precision in performing a task comes with subtle movements at low velocities that the robot can emulate it by imposing high impedance. Conversely, low impedance is of interest when one needs to perform large movements at high velocities [15], [16], [17], [18], [19], [20], [21]. Therefore, researchers have regulated the desired robot impedance in each task based on the end-effector velocity without requiring any force measurement (as stated in Table I). Moreover, in some applications such as robot-assisted welding, since the welder needs to carry the torch through the welding line, there is no pre-specified position trajectory for the end-effector while its velocity has to be controlled. In addition, mitigating the uncontrolled vibrations in robot-assisted welding is achievable by setting large damping for the torch movement that is only favourable during welding operation at a slow speed. However, when welding is not in progress, a relatively high damping value causes difficulty in transporting the torch from one point to another. Due to the lack of reference position and to ease the manipulation of the torch between the welding phases, the velocity-dependent VIC was adopted in [22], [23]. In a similar fashion, the admissible region of damping variation was obtained experimentally in [15] in order to enhance the accuracy and execution time in a drawing task. Accordingly, an exponential function was adopted to change the robot damping matrix $\mathbf{B}_x^d$ within the obtained region in terms of the robot end-effector's absolute velocity. Ikeura *et al.* [24] proposed a switching-type impedance control method for a cooperative task between human and a robot based on a velocity threshold ($\mathbf{v}_0$) as

$$\begin{cases}\mathbf{f}_e = \mathbf{M}_x^d\ddot{\mathbf{x}} + \mathbf{B}_x^{d_1}\dot{\mathbf{x}}, & \dot{\mathbf{x}} \prec \mathbf{v}_0\\ \mathbf{f}_e = \mathbf{M}_x^d\ddot{\mathbf{x}} + \mathbf{B}_x^{d_2}\dot{\mathbf{x}}, & \dot{\mathbf{x}} \succeq \mathbf{v}_0\end{cases} \tag{6}$$

where the vectors $\mathbf{f}_e$ and $\mathbf{x}$ are the force and position of the end-effector, and matrices $\mathbf{B}_x^{d_1}$, $\mathbf{B}_x^{d_2}$, and $\mathbf{M}_x^d$ are the high damping parameter, low damping parameter, and inertia, respectively. In this method, the model parameters were approximated from users' force and position data recorded experimentally. According to Eq. (6), for velocities below $\mathbf{v}_0$, the desired damping parameter is set to its higher level $\mathbf{B}_x^{d_1}$, and when the end-effector velocity exceeds the threshold $\mathbf{v}_0$, the desired damping parameter switches to its lower magnitude $\mathbf{B}_x^{d_2}$ to increase the movability of the robot. In their later work [16], they solved the discontinuity problem for the desired damping parameter by employing an exponential function for a smooth variation between $\mathbf{B}_x^{d_1}$ and $\mathbf{B}_x^{d_2}$.

B. Force-Based Approaches

Control of the interaction force between robot and environment is vital, notably in some tasks that need a certain level of force for their execution such as in grinding [70], assembling [71], deburring [72] and surgery [73]. Using typical impedance controllers, one can control the interaction force indirectly by regulating the robot position and choosing the desired impedance in compliance with the environmental structure [74] as expressed in Table I. However, uncertainties in robot/environment dynamics and kinematics can render a poor indirect force control. Consequently, a force-based variable impedance controller was designed in [14] for direct HRI force control assuming its continuous differentiability. Having (4) as the desired impedance in which $\mathbf{M}_x^d$, $\mathbf{B}_x^d$ and

	Methodology	Objective	Requirements	Benefits	Drawbacks	References
Impedance Variation	Velocity-based	Adjusting robot impedance based on its end-effector velocity at each portion of task	• Position data	• Providing both slow (precise) and high-speed (free) movements • No need to force measurement	• Lack of analytical stability proof	[24], [20], [16], [19], [21], [18], [23], [17], [22], [15]
	Force-based	Interaction force control via impedance variation	• Position data • Force data	• Compliant interaction by direct force control	• Not appropriate for precise positioning and velocity-based tasks • Not appropriate in the presence of robot/environment modeling uncertainties	[14], [25], [26], [27], [28], [29]
	EMG-based	Replicating human impedance (obtained from EMG signals) in each task for the robot	• Position data • EMG data	• Bio-inspired impedance variation by estimation of human limb stiffness	• Requiring rich and diverse data • Lack of stability consideration • Excluding damping and inertia in human and desired robot impedance analyses	[30], [31], [32], [33], [34], [35], [36]
	Stability-based	Guaranteeing a stable physical HRI while varying the impedance, considering the robot and human dynamics (in some cases)	• Position data	• Having stable and safe HRI • No need to force measurement • For non-passive humans (in some cases)	• More conservative on the robot stability rather than having a compliant performance (with specific impedance values) • Model-based strategies (requiring the robot and/or human dynamic structure, but can be uncertain)	[37], [38], [38], [39], [40], [41], [42], [43], [44], [45], [46], [47], [48], [49], [50]
Impedance Learning	LFD-based	Obtaining mean trajectory and adjusting impedance based on Gaussian approximations	• Position data • Force / EMG data	• Model-free algorithms (no need to human and robot models)	• Lack of stability guarantee • Requiring demonstration steps (for offline learning)	[51], [52], [53], [54], [55], [56], [57], [34], [58], [59]
	Optimization-based	Identifying appropriate impedance parameters based on considered human and impedance models	• Position data • Force data	• No need to know robot dynamics • Uncertainty on human dynamic parameters	• Lack of robot stability guarantee • Requiring a structure for human dynamics	[60], [61], [62], [63]
	AI-based	Emulating the decision making process and the physical behavior pattern of human (for different task specifications such as precise positioning and velocity adjustment)	• Position data • Force data	• Model-free algorithms (no need to human and robot models) • Powerful mathematical tools to realize intelligent human-robot collaboration in complicated tasks (high-level skill learning)	• Lack of stability proof • Having considerable computation costs and training cycles (in complex algorithms)	[64], [65], [66], [67], [68], [69]

TABLE I
CHARACTERISTICS, REQUIREMENTS AND FEATURES OF STUDIED IMPEDANCE VARIATION AND LEARNING METHODS

$\mathbf{K}_x^d$ are unknown, a controlled version of this impedance model was defined to regulate the contact force as

$$\hat{\mathbf{M}}_x^d\ddot{\tilde{\mathbf{x}}} + \hat{\mathbf{B}}_x^d\dot{\tilde{\mathbf{x}}} + \hat{\mathbf{K}}_x^d\tilde{\mathbf{x}} = \mathbf{f}_d - \mathbf{K}_f\dot{\tilde{\mathbf{f}}} \tag{7}$$

where $\tilde{\mathbf{f}} = \mathbf{f}_d - \mathbf{f}_e$ and $\tilde{\mathbf{x}} = \mathbf{x} - \mathbf{x}_0$. $\hat{\mathbf{M}}_x^d$, $\hat{\mathbf{B}}_x^d$ and $\hat{\mathbf{K}}_x^d$ are the implemented time-varying impedance parameters. Also, $\mathbf{f}_d \in \mathbb{R}^{m\times 1}$ is the desired contact force and $\mathbf{K}_f \in \mathbb{R}^{m\times m}$ is a gain matrix of the force error term. Based on Eqs. (4) and (7), and denoting $\tilde{\mathbf{M}}_x^d = \mathbf{M}_x^d - \hat{\mathbf{M}}_x^d$, $\tilde{\mathbf{B}}_x^d = \mathbf{B}_x^d - \hat{\mathbf{B}}_x^d$ and $\tilde{\mathbf{K}}_x^d = \mathbf{K}_x^d - \hat{\mathbf{K}}_x^d$, one can write:

$$\dot{\tilde{\mathbf{f}}} = \mathbf{K}_f^{-1}\tilde{\mathbf{f}} + \mathbf{K}_f^{-1}\mathbf{Y}\left(\tilde{\mathbf{x}},\dot{\tilde{\mathbf{x}}},\ddot{\tilde{\mathbf{x}}}\right)\boldsymbol{\theta}\left(\tilde{\mathbf{M}}_x^d,\tilde{\mathbf{B}}_x^d,\tilde{\mathbf{K}}_x^d\right) \tag{8}$$

where $\mathbf{Y}(.) \in \mathbb{R}^{m\times 3m}$ and $\boldsymbol{\theta}(.) \in \mathbb{R}^{3m\times 1}$ are the regressor position-error matrix and the unknown impedance-error vector, respectively. Equation (8) is obtained given that the Lagrangian dynamics is linearly parameterizable. Choosing the Lyapunov function as $V = \tilde{\mathbf{f}}^T\mathbf{P}\tilde{\mathbf{f}} + \boldsymbol{\theta}^T\boldsymbol{\Gamma}\boldsymbol{\theta}$, where $\mathbf{P}$ and $\boldsymbol{\Gamma}$ are positive definite matrices, its time derivative was obtained as

$$\begin{aligned}\dot{V} = \tilde{\mathbf{f}}^T\left(\mathbf{K}_f^{-T}\mathbf{P} + \mathbf{P}\mathbf{K}_f^{-1}\right)\tilde{\mathbf{f}} \\ + 2\left(\dot{\boldsymbol{\theta}}^T\boldsymbol{\Gamma}\boldsymbol{\theta} + \tilde{\mathbf{f}}^T\mathbf{P}\mathbf{K}_f^{-1}\mathbf{Y}\boldsymbol{\theta}\right)\end{aligned} \tag{9}$$

Now, if $\mathbf{P}$, $\boldsymbol{\Gamma}$ and $\boldsymbol{\theta}$ satisfy the following conditions

$$\begin{aligned}\mathbf{K}_f^{-T}\mathbf{P} + \mathbf{P}\mathbf{K}_f^{-1} &= \mathbf{Q}_0 \\ \boldsymbol{\theta}^T\boldsymbol{\Gamma}\boldsymbol{\theta} + \tilde{\mathbf{f}}^T\mathbf{P}\mathbf{K}_f^{-1}\mathbf{Y}\boldsymbol{\theta} &= 0\end{aligned} \tag{10}$$

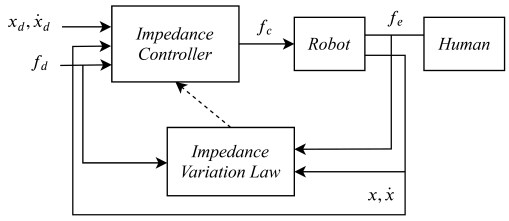

Fig. 1. Schematic diagram of force-based variable impedance controller in the end-effector's Cartesian space

where $\mathbf{Q}_0$ is a negative semi-definite matrix, then $\dot{V} = \tilde{\mathbf{f}}^T\mathbf{Q}_0\tilde{\mathbf{f}} \leq 0$. Thereby, the closed-loop system of this force-based variable impedance controller [14] was proven to be stable. Given (10), the state-dependent adaptation law for $\hat{\mathbf{M}}_x^d$, $\hat{\mathbf{B}}_x^d$, $\hat{\mathbf{K}}_x^d$ was defined as

$$\dot{\boldsymbol{\theta}} = -\left(\tilde{\mathbf{f}}^T\mathbf{P}\mathbf{K}_f^{-1}\mathbf{Y}\boldsymbol{\Gamma}^{-1}\right)^T = -\boldsymbol{\Gamma}^{-1}\mathbf{Y}^T\mathbf{K}_f^{-T}\mathbf{P}\tilde{\mathbf{f}} \tag{11}$$

and since $V > 0$ and $\dot{V} \leq 0$, $\tilde{\mathbf{f}} \to 0$ is concluded (i.e., $\mathbf{f}_d \to \mathbf{f}_e$). The schematic diagram of the proposed force-based variable impedance control method [14] in the end-effector's Cartesian space is shown in Fig. 1. As mentioned earlier in Section III-A, it is of interest in some applications to decrease the damping when the force and velocity are in the same direction (acceleration magnitude is considerable), and

vice versa. In line with this rationale, a variable impedance controller was put forward in [29] with the following damping regulation:

$$\mathbf{B}_x^d(t) = -\boldsymbol{\alpha}\,\mathrm{diag}(\mathbf{f}_e)\,\mathrm{diag}\left(\mathrm{sgn}(\dot{\mathbf{x}})\right) + \mathbf{B}_x^0 \tag{12}$$

where $\mathbf{B}_x^0$ is a constant diagonal matrix as the initial damping value. The corresponding desired dynamic behavior of the end-effector is described by (4) with null stiffness parameter. In [28], the optimal damping and inertia of the target impedance were also determined based upon minimization of the upper bound of contact forces (for a certain range of human inertia and stiffness).

It is worth mentioning that most of the force-based impedance variations have not been designed for precise positioning and velocity-based tasks in the presence of modeling uncertainties. In [26] and [27], the desired damping parameter was altered proportionally to the estimated stiffness of the human arm in low velocities.

C. EMG-based Approaches

Electromyography (EMG) is a procedure to scrutinize the activity of muscles and the nerve cells that innervate them [75]. Motor neurons transmit electrical signals to contract muscles which can be received by deploying EMG electrodes on the surface of muscles [30], [31], [33], [34], [35], [32]. In [30], the concept of tele-impedance was introduced for HRI, in which the desired endpoint stiffness of the robot is adjusted in real-time using the human arm stiffness estimated through analyzing EMG signals of eight muscles acting on the shoulder and elbow joints. For this purpose, a linear mapping between the human force/stiffness and the muscular activation/coactivation was formulated in [30] as

$$\begin{bmatrix}\mathbf{f}_e \\ \mathbf{k}_x^d\end{bmatrix} = \begin{bmatrix}\mathbf{T}_f \\ \mathbf{T}_k\end{bmatrix}\mathbf{u}^{EMG} + \begin{bmatrix}0 \\ \mathbf{k}_x^0\end{bmatrix} \tag{13}$$

where $\mathbf{k}_x^d \in \mathbb{R}^3$ and $\mathbf{f}_e \in \mathbb{R}^3$ are the endpoint stiffness and force vectors, respectively. Also, $\mathbf{k}_x^0$ is the stiffness in relaxed arm conditions, and $\mathbf{u}^{EMG} \in \mathbb{R}^n$ is the vector of eight muscles activities obtained from EMG signals. The matrices $\mathbf{T}_k$ and $\mathbf{T}_f$ were experimentally identified which entails precise measurements of $\mathbf{k}_x^d$ and $\mathbf{f}_e$ through enough diverse data samples. The obtained values for the human stiffness $\mathbf{k}_x^d$ were considered as inputs for the endpoint impedance controller of the robot in [76], [77]. In another study [36], the damping level of the robot's admittance controller was adjusted during HRI based on estimating the human arm endpoint stiffness in terms of the co-contraction of antagonist muscles. As mentioned in Table I, some disadvantages of the above-mentioned EMG-based impedance variations are the requirement of rich and varied data, lack of robot stability consideration, and the exclusion of damping and inertia of the human in robot impedance shaping.

D. Stability-based Approaches

In VIC strategies, the variation of impedance parameters may violate the stability conditions. Therefore, it is of paramount importance to strike a balance between achieving a desirable performance (impedance-based compliance) and ensuring robot stability, especially for those applications such as medical robotics where human safety is a significant concern (as pointed out in Table I). Suppose a robot-assisted needle inserting system [78], [79] for surgical tasks in which the robot instability may inflict serious tissue injuries on the patient. In some applications like robotic surgery [80], it is hard to mount a force sensor at the tip of robot end-effector due to some design limitations related to robot size or its mobility/dexterity. As suggested in [37], a direct feedback from the interaction force $\mathbf{f}_e$ can be avoided by setting the same inertia for the desired impedance model (4) as that of the robot ($\mathbf{M}_x^d = \mathbf{M}_x$). Accordingly, the desired HRI impedance dynamics was selected in [40], [38] as

$$\mathbf{M}_x\ddot{\tilde{\mathbf{x}}} + \left(\mathbf{B}_x^d + \mathbf{C}_x\right)\dot{\tilde{\mathbf{x}}} + \mathbf{K}_x^d\tilde{\mathbf{x}} = \mathbf{f}_e \tag{14}$$

where $\tilde{\mathbf{x}} = \mathbf{x} - \mathbf{x}_0$. Defining the following storage function

$$V\left(\tilde{\mathbf{x}}, \dot{\tilde{\mathbf{x}}}\right) = \frac{1}{2}\dot{\tilde{\mathbf{x}}}^T\mathbf{M}_x\dot{\tilde{\mathbf{x}}} + \frac{1}{2}\tilde{\mathbf{x}}^T\mathbf{K}_x^d\tilde{\mathbf{x}} \tag{15}$$

and substituting $\ddot{\tilde{\mathbf{x}}}$ from (14) into the time derivative of the above-mentioned storage function, yields that the system in (14) is passive with respect to the pair $\left(\mathbf{f}_e, \dot{\tilde{\mathbf{x}}}\right)$ since $\dot{V}$ culminates in

$$\begin{aligned}\dot{V} &= \dot{\tilde{\mathbf{x}}}^T\mathbf{f}_e - \dot{\tilde{\mathbf{x}}}^T\mathbf{B}_x^d\tilde{\mathbf{x}} \le \dot{\tilde{\mathbf{x}}}^T\mathbf{f}_e \\ V(t) - V(0) &\le \int_0^t \dot{\tilde{\mathbf{x}}}^T(\tau)\mathbf{f}_e(\tau)d\tau\end{aligned} \tag{16}$$

As a result, in free motions and physical contacts with passive environments, stable robot behavior is ensured. However, an impedance model is needed that could take on a surgeon's actions, e.g., stiffness alteration (characterized by state-dependent time-varying $\mathbf{K}_x^d$) during a puncturing task [81], while preserving the robot stability. In this situation, the time derivative of the storage function (15) was obtained as [38]

$$\dot{V} = \dot{\tilde{\mathbf{x}}}^T\mathbf{f}_e + \left[\frac{1}{2}\tilde{\mathbf{x}}^T\dot{\mathbf{K}}_x^d(t)\tilde{\mathbf{x}} - \dot{\tilde{\mathbf{x}}}^T\mathbf{B}_x^d\dot{\tilde{\mathbf{x}}}\right] \tag{17}$$

which shows that the stiffness variability renders the passivity condition (16) no longer guaranteed. Consequently, tank-based impedance control strategies were developed to provide a variable stiffness while preserving the robot passivity for a stable HRI [38], [39], [40], [43]. The main idea of the tank-based approaches is to create a reservoir for storing the energy being dissipated by the controlled system. To this end, the tank-based control law [38] was proposed as

$$\mathbf{f}_c = \mathbf{g}_x + \mathbf{M}_x\ddot{\mathbf{x}}_0 + \mathbf{C}_x\dot{\mathbf{x}}_0 - \mathbf{B}_x^d\dot{\tilde{\mathbf{x}}} - \mathbf{K}_x^c\tilde{\mathbf{x}} + \boldsymbol{\omega}x_t \tag{18}$$

where $\mathbf{K}_x^c$ is a constant stiffness and $x_t \in \mathbb{R}$ is the state associated with the tank system governed by

$$\begin{cases}\dot{x}_t = \frac{\sigma}{x_t}\left(\dot{\tilde{\mathbf{x}}}^T\mathbf{B}_x^d\dot{\tilde{\mathbf{x}}}\right) - \boldsymbol{\omega}^T\dot{\tilde{\mathbf{x}}} \\ \mathbf{y} = \left(\dot{\tilde{\mathbf{x}}}^T x_t\right)^T\end{cases} \tag{19}$$

such that

$$T\left(x_t\right) = \frac{1}{2}x_t^2 \tag{20}$$

is the energy stored in the tank which can be exploited for deploying the variable stiffness $\mathbf{K}_x^v(t)$. Thereby, the gain $\boldsymbol{\omega}$ in Eq. (18) was determined by

$$\boldsymbol{\omega}(t) = \begin{cases} -\frac{\mathbf{K}_x^v(t)\tilde{\mathbf{x}}}{x_t} & if \;\; T(x_t) > \varepsilon \\ 0 & \text{otherwise} \end{cases} \tag{21}$$

which controls the exchange of energy between the main impedance model (14) and the tank (19). Also, ε in (21) is the minimum threshold up to which the tank is allowed to be used up. Applying the controller (18) to the robotic system (2), the closed-loop dynamics yielded as

$$\mathbf{M}_x\ddot{\tilde{\mathbf{x}}} + \left(\mathbf{B}_x^d + \mathbf{C}_x\right)\dot{\tilde{\mathbf{x}}} + \mathbf{K}_x^c\tilde{\mathbf{x}} - \boldsymbol{\omega}x_t = \mathbf{f}_e \tag{22}$$

Substituting (21) into (18), the desired stiffness is equal to $\mathbf{K}_x^c + \mathbf{K}_x^v$ when $T(x_t) > \varepsilon$ or equal to $\mathbf{K}_x^c$ when $T(x_t) \leq \varepsilon$. Moreover, σ in (19) regulates the level (based on practical considerations [82]) up to which the energy can be stored in the tank that is according to the following rule

$$\sigma = \begin{cases} 1 & if \;\; T(x_t) \leq \overline{T} \\ 0 & \text{otherwise} \end{cases} \tag{23}$$

where $\overline{T}$ is the maximum tank capacity. Considering that the robot's closed-loop dynamics (22) is energetically coupled with the tank system through the input $\boldsymbol{\omega}(t)$, the overall energy of the robotic system was given by

$$V\left(\tilde{\mathbf{x}}, \dot{\tilde{\mathbf{x}}}\right) = \frac{1}{2}\dot{\tilde{\mathbf{x}}}^T\mathbf{M}_x\dot{\tilde{\mathbf{x}}} + \frac{1}{2}\tilde{\mathbf{x}}^T\mathbf{K}_x^c\tilde{\mathbf{x}} \tag{24}$$

where its derivative is

$$\dot{V} = \dot{\tilde{\mathbf{x}}}^T\mathbf{f}_e - \dot{\tilde{\mathbf{x}}}^T\mathbf{B}_x^d\dot{\tilde{\mathbf{x}}} + \dot{\tilde{\mathbf{x}}}^T\boldsymbol{\omega}x_t \tag{25}$$

Having $\dot{T} = x_t\dot{x}_t = \sigma\left(\dot{\tilde{\mathbf{x}}}^T\mathbf{B}_x^d\dot{\tilde{\mathbf{x}}}\right) - x_t\boldsymbol{\omega}^T\dot{\tilde{\mathbf{x}}}$ and adding it to $\dot{V}$ in (25) implies that the energy dissipated by the implemented impedance controller is stored in the tank until it reaches its upper limit $\overline{T}$, such that this energy is injected from the tank to the robot via the control law (18) and $\boldsymbol{\omega}(t)$ in (21). Now, taking $W\left(\tilde{\mathbf{x}}, \dot{\tilde{\mathbf{x}}}, x_t\right) = V\left(\tilde{\mathbf{x}}, \dot{\tilde{\mathbf{x}}}\right) + T(x_t)$ into account as the storage function of the total coupled system, its derivative was obtained as

$$\dot{W} = \dot{\tilde{\mathbf{x}}}^T\mathbf{f}_e + (\sigma - 1)\dot{\tilde{\mathbf{x}}}^T\mathbf{B}_x^d\dot{\tilde{\mathbf{x}}} \tag{26}$$

Regarding $\sigma \in [0, 1]$, one can write $\dot{W} \leq \dot{\tilde{\mathbf{x}}}^T\mathbf{f}_e$, and thus:

$$W(t) - W(0) \leq \int_0^t \dot{\tilde{\mathbf{x}}}^T(\tau)\mathbf{f}_e(\tau)d\tau \tag{27}$$

which means that the coupled system is passive concerning the input-output pair of $\mathbf{f}_e$ and $\dot{\tilde{\mathbf{x}}}$. In [41], a state-independent stability condition was proposed for varying stiffness and damping, which is of practical importance for verifying the stability conditions offline before any execution of the task. Having (1) when $\boldsymbol{\tau}_f = 0$ as the dynamics of the robot manipulator, and (5) as the desired closed-loop dynamic relationship, the following controller was designed in [41]:

$$\boldsymbol{\tau}_c = \mathbf{M}_q\boldsymbol{\nu} + \mathbf{C}_q\dot{\mathbf{q}} + \mathbf{g}_q - \boldsymbol{\tau}_e \tag{28}$$

where

$$\boldsymbol{\nu} = \ddot{\mathbf{q}}_d + \mathbf{H}^{-1}\left(-\mathbf{B}_q^d\dot{\tilde{\mathbf{q}}} - \mathbf{K}_q^d\left(\mathbf{q} - \dot{\mathbf{q}}_d\right) + \boldsymbol{\tau}_e\right) \tag{29}$$

in which $\mathbf{H} = \mathbf{M}_q^d$ is a constant positive definite matrix while $\mathbf{B}_q^d$ and $\mathbf{K}_q^d$ are time-varying impedance parameters. The following Lyapunov function was suggested to analyze the robot stability:

$$V(\tilde{\mathbf{q}}, \dot{\tilde{\mathbf{q}}}, t) = \frac{\left(\dot{\tilde{\mathbf{q}}} + \alpha\tilde{\mathbf{q}}\right)^T\mathbf{H}\left(\dot{\tilde{\mathbf{q}}} + \alpha\tilde{\mathbf{q}}\right)}{2} + \frac{\tilde{\mathbf{q}}^T\boldsymbol{\beta}(t)\tilde{\mathbf{q}}}{2} \tag{30}$$

where $\boldsymbol{\beta}(t)$ is a positive semi-definite and continuously differentiable matrix defined as

$$\boldsymbol{\beta}(t) = \mathbf{K}_q^d(t) + \alpha\mathbf{B}_q^d(t) - \alpha^2\mathbf{H} \tag{31}$$

in which α is a positive constant. This function allowed them to establish sufficient constraints on the stability independently of system states. Differentiating (30) with respect to the time, and substituting the closed-loop dynamics (5) with $\boldsymbol{\tau}_e = 0$ into it yields

$$\begin{aligned} \dot{V}(\tilde{\mathbf{q}}, \dot{\tilde{\mathbf{q}}}, t) = {} & \dot{\tilde{\mathbf{q}}}^T\left(\alpha\mathbf{H} - \mathbf{B}_q^d(t)\right)\dot{\tilde{\mathbf{q}}} \\ & + \frac{1}{2}\tilde{\mathbf{q}}^T\left(\dot{\mathbf{K}}_q^d(t) + \alpha\dot{\mathbf{B}}_q^d(t) - 2\alpha\mathbf{K}_q^d(t)\right)\tilde{\mathbf{q}} \end{aligned} \tag{32}$$

Thereby, $\dot{V}(\tilde{\mathbf{q}}, \dot{\tilde{\mathbf{q}}}, t) \leq 0$ is satisfied when

1) $\alpha\mathbf{H} - \mathbf{B}_q^d(t)$ is negative semi-definite, and
2) $\dot{\mathbf{K}}_q^d(t) + \alpha\dot{\mathbf{B}}_q^d(t) - 2\alpha\mathbf{K}_q^d(t)$ is negative semi-definite

and accordingly it can be concluded that the impedance dynamics (5) in the absence of physical interaction ($\boldsymbol{\tau}_e = 0$) is globally uniformly stable.

In another study [44], Eq. (5) was employed and the desired variable impedance dynamics $\mathbf{M}_q^d$, $\mathbf{B}_q^d$ and $\mathbf{K}_q^d$ were considered to be diagonal positive definite matrices having bounded elements, and the last two matrices were considered to be time-varying. Defining $\mathbf{M}_d = \mathbf{M}_q^d$, $\overline{\boldsymbol{\tau}}_e = \mathbf{M}_d^{-1}\boldsymbol{\tau}_e$, $\boldsymbol{\alpha} = \mathbf{q}_d - \mathbf{q}$, $\overline{\mathbf{B}}_d(t) = \text{diag}\{\overline{b}_{ii}(t)\} = \mathbf{M}_d^{-1}\mathbf{B}_q^d(t)$ and $\overline{\mathbf{K}}_d(t) = \text{diag}\{\overline{k}_{ii}(t)\} = \mathbf{M}_d^{-1}\mathbf{K}_q^d(t)$, the desired dynamics was expressed in linear time-varying (LTV) systems' format as

$$\begin{bmatrix} \dot{\boldsymbol{\alpha}} \\ \ddot{\boldsymbol{\alpha}} \end{bmatrix} = \begin{bmatrix} \mathbf{0} & \mathbf{I} \\ -\overline{\mathbf{K}}_d(t) & -\overline{\mathbf{B}}_d(t) \end{bmatrix}\begin{bmatrix} \boldsymbol{\alpha} \\ \dot{\boldsymbol{\alpha}} \end{bmatrix} + \begin{bmatrix} \overline{\mathbf{0}} \\ \overline{\boldsymbol{\tau}}_e \end{bmatrix} \tag{33}$$

which was shown equivalently as

$$\begin{bmatrix} \dot{\alpha}_i \\ \ddot{\alpha}_i \end{bmatrix} = \begin{bmatrix} 0 & 1 \\ -\overline{k}_{ii}(t) & -\overline{b}_{ii}(t) \end{bmatrix}\begin{bmatrix} \alpha_i \\ \dot{\alpha}_i \end{bmatrix} + \begin{bmatrix} 0 \\ \overline{\tau}_{e_i} \end{bmatrix} \quad \text{for } i = 1, 2, \ldots n \tag{34}$$

Then, some constraints are given for stiffness and damping coefficients concerning the system stability as the following relations:

$$\begin{cases} \exists\, \beta_1 \in \mathbb{R} > 0; & \overline{k}_{ii}(t) \geq \beta_1 \\ \exists\, \beta_2, \beta_3 \in \mathbb{R} > 0; & \beta_2 \leq \frac{\overline{b}_{ii}(t) + 0.5\frac{\dot{\overline{k}}_{ii}(t)}{\overline{k}_{ii}(t)}}{\sqrt{\overline{k}_{ii}(t)}} \leq \beta_3 \end{cases} \tag{35}$$

It was demonstrated that besides the above conditions, if $\overline{k}_{ii}(t) > 0$ and $\lambda_1(t)$, $\lambda_2 > 0$ such that $\exp(-\int_{t_0}^t \sqrt{\overline{k}_{ii}(t)}dt) \leq \lambda_1(t_0)e^{-\lambda_2 t}$, then the system described by (34) with $\overline{\tau}_{e_i}$ being zero is uniformly asymptotically stable (UAS). Note that an LTV system is uniformly exponentially stable (UES) if and only if it is UAS [83]. As

a result, the system (34) with zero interaction force is UES, i.e.:

$$\exists\ \mu, k(t) > 0;\ \ ||\mathbf{\Phi}_i(t, t_0)|| \leq k(t_0)e^{-\mu(t-t_0)},\ t \geq t_0 \quad (36)$$

where $\mathbf{\Phi}_i(t, t_0)$ is the state transition matrix of the system (34). By satisfying the above conditions, the desired variable impedance dynamics is exponentially stable, and the robot's position, velocity, and acceleration in (5) are all bounded, if the interaction force is bounded. In [42], a similar VIC method was employed to improve HRI by imposing stability-based conditions on varying impedance parameters, where the robot model was approximated based on uncertainty-disturbance estimator (UDE) [84]. Although the above methods enhanced the human safety via guaranteed stability without any force measurement, they can pose digression from the desired time-varying impedance, which implies a trade-off between stability and performance (as stated in Table I).

In other methods, the environment (human) behavior was modeled to be non-passive with unknown parameters, while the controller ensured the stability of the robot's physical interactions by adopting appropriate impedance adaptations. As summarized in Table I, these beneficial aspects come true without any interaction force measurement, having structures of the robot and human behavior. Accordingly, it was demonstrated that the robot would adjust its impedance in response to various high- and low-frequency external disturbances. The possible applications of these strategies were mentioned service robotics, health care, manufacturing, construction, entertainment and agriculture where the environment behavior can be non-passive with unknown impedance and force [45], [47], [49].

A human-like impedance adaptation strategy was proposed and tested in [45], [46] to provide a flexible physical interaction between the robot and human while guaranteeing the robot's stability via a comprehensive Lyapunov analysis. The following three-term model was considered for the physical HRI torque:

$$\boldsymbol{\tau}_e(t) = \boldsymbol{\tau}(t) + \mathbf{K}_q(t)\mathbf{e}(t) + \mathbf{B}_q(t)\dot{\mathbf{e}}(t) \quad (37)$$

where the first term on the right-hand side is a feedforward torque, and the second and third terms are stiffness-based and damping-based torques of the human in physical interactions. The position and velocity errors were also defined as $\mathbf{e}(t) = \mathbf{q}(t) - \mathbf{q}_d(t)$ and $\dot{\mathbf{e}}(t) = \dot{\mathbf{q}}(t) - \dot{\mathbf{q}}_d(t)$.

In this bio-inspired adaptation method [45], optimum impedance parameters and feed-forward force of HRI were updated online without any force measurement through employing adaptation laws inspired by human behavior [85]. This resulted in robot stability in the execution of physical tasks while the human environment has unknown interaction. The state-dependent impedance update rules used to estimate the variations of feedforward force, stiffness and damping elements (characterized by δ) as [45], [47]

$$\delta\hat{\boldsymbol{\tau}}_e(t) = \mathbf{Q}_\tau\left(\boldsymbol{\epsilon}(t) - \gamma(t)\hat{\boldsymbol{\tau}}_e(t)\right) \quad (38)$$

$$\delta\hat{\mathbf{K}}_q(t) = \mathbf{Q}_K\left(\boldsymbol{\epsilon}(t)\mathbf{e}^T(t) - \gamma(t)\hat{\mathbf{K}}_q(t)\right) \quad (39)$$

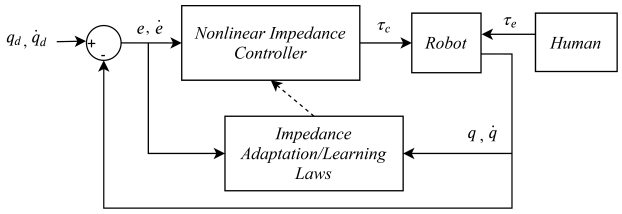

Fig. 2. Schematic diagram of stability-based impedance adaptation methods the robot's joint space

$$\delta\hat{\mathbf{B}}_q(t) = \mathbf{Q}_B\left(\boldsymbol{\epsilon}(t)\dot{\mathbf{e}}^T(t) - \gamma(t)\hat{\mathbf{B}}_q(t)\right) \quad (40)$$

where the superscript $\hat{}$ is the estimation sign, and $\mathbf{Q}_\tau$, $\mathbf{Q}_K$ and $\mathbf{Q}_B$ are positive definite constant matrices as the adaptation gains, and $\gamma(t) = \frac{a}{1+b\|\boldsymbol{\epsilon}(t)\|^2}$ is the forgetting factor of this adaptation in which a and b are positive constants. Also, $\boldsymbol{\epsilon}(t) = \dot{\mathbf{e}} + \kappa\mathbf{e}$ (with $\kappa > 0$) was defined as the tracking error dynamics in terms of the position and velocity errors ($\mathbf{e}$ and $\dot{\mathbf{e}}$). A schematic diagram of this stability-based impedance adaptation control in the robot's joint space is shown in Fig. 2.

By defining a Lyapunov function and formulating the impedance adaptation laws (38)-(40) in terms of tracking error to compensate for HRI torque, a bounded deviation from the desired trajectory is permitted to ensure stability and compliant behavior. The corresponding Lyapunov function $V(t) = V_p(t) + V_c(t)$ was defined as

$$\begin{aligned} V_p(t) =& \frac{1}{2}\boldsymbol{\epsilon}^T(t)\mathbf{M}_q\boldsymbol{\epsilon}(t) \\ V_c(t) =& \frac{1}{2}\int_{t-T_s}^{t}\Big[\tilde{\boldsymbol{\tau}}_e^T(\rho)\mathbf{Q}_\tau^{-1}\tilde{\boldsymbol{\tau}}_e(\rho) \\ &+\text{vec}(\tilde{\mathbf{K}}_q(\rho))^T\mathbf{Q}_K^{-1}\text{vec}(\tilde{\mathbf{K}}_q(\rho)) \\ &+\text{vec}(\tilde{\mathbf{B}}_q(\rho))^T\mathbf{Q}_B^{-1}\text{vec}(\tilde{\mathbf{B}}_q(\rho))\Big]\,d\rho \end{aligned} \quad (41)$$

where T_s is sampling time for execution of the controller, and vec(.) is the column vectorization operator.

It is notable that in [48], the strategy for impedance adaptation [45] was modified by taping into the online stiffness estimation of the human arm based on EMG signals, which was tested on the Baxter robot in a teleoperation system. Moreover, an extended version of this method [45] was proposed in [49] for trajectory adaptation to enhance the biomimetic autonomy of the robot via revising the desired trajectory in hard contacts with obstacles. This approach was inspired by humans behavior that change their path for obstacle avoidance instinctively in addition to adapting their limb impedance when running into rigid obstacles. For this purpose, the unknown desired trajectory and its estimated reference one were defined respectively as

$$\begin{aligned} \boldsymbol{\zeta}_d =& \mathbf{K}_q^*\mathbf{q}_d + \mathbf{B}_q^*\dot{\mathbf{q}}_d \\ \boldsymbol{\zeta}_r =& \mathbf{K}_q\mathbf{q}_r + \mathbf{B}_q\dot{\mathbf{q}}_r \end{aligned} \quad (42)$$

where $\mathbf{K}_q^*$ and $\mathbf{B}_q^*$ are the unknown stiffness and damping coefficients of the environment, respectively. Moreover, $\mathbf{K}_q$ and $\mathbf{B}_q$ are the employed stiffness and damping parameters

of the robot impedance being updated via the adaptation laws (39) and (40), respectively. In this regard, they obtained the following update rule for initially specified trajectory in terms of the difference between the desired $\boldsymbol{\tau}_d$ and current $\boldsymbol{\tau}_e$ feedforward forces of the interaction as

$$\delta\boldsymbol{\zeta}_r(t) = \mathbf{L}^{-T}\mathbf{Q}_r(\boldsymbol{\tau}_d(t) - \boldsymbol{\tau}_e(t) - \boldsymbol{\zeta}_r(t)) \tag{43}$$

in which $\mathbf{L}$ and $\mathbf{Q}_r$ are positive definite constant gain matrices. As a result of this modification, the previous adaptation law for the feedforward interaction force (38) proposed in [45] was also amended in terms of the recent trajectory variation rule (43) as

$$\delta\boldsymbol{\tau}_e(t) = \mathbf{Q}_\tau(\boldsymbol{\epsilon}(t) - \gamma(t)\boldsymbol{\tau}_e(t) + \mathbf{Q}_r^T\delta\boldsymbol{\zeta}_r(t)) \tag{44}$$

while the controller design in this strategy [49] is similar to the one in [45] as illustrated in Fig. 2. In other words, the force and trajectory adaptation rules in this study were coupled to enhance the robot stability and compliance. This was proven via the following Lyapunov function:

$$V(t) = V_r(t) + V_c(t) + V_p(t) \tag{45}$$

where $V_p(t)$ and $V_c(t)$ are defined in [49] the same as the ones presented in [45] by Eq. (41). However, $V_r(t)$ was suggested as follows:

$$V_r(t) = \frac{1}{2}\int_{t-T_s}^{t}(\boldsymbol{\zeta}_r(\rho)-\boldsymbol{\zeta}_d(\rho))^T\mathbf{Q}_r^T(\boldsymbol{\zeta}_r(\rho)-\boldsymbol{\zeta}_d(\rho))\,d\rho \tag{46}$$

As seen in (45) and (46), this Lyapunov function was integrated with an additional quadratic function in comparison with (41) in terms of the difference between $\boldsymbol{\zeta}_d$ and $\boldsymbol{\zeta}_r$ trajectories. Note that other studies [86] were performed on the trajectory adaptation or online path planning for obstacle avoidance but without changing the impedance parameters during task execution.

In another study [50], the human interaction force was modeled by spring and damper elements (without any feedforward force component that was considered in [45]):

$$\boldsymbol{\tau}_e = \mathbf{K}_h(t)\mathbf{e}(t) + \mathbf{B}_h(t)\dot{\mathbf{q}}(t) \tag{47}$$

in which estimations of $\mathbf{K}_h(t)$ and $\mathbf{B}_h(t)$ were formulated with similar impedance adaptation laws mentioned in Eqs. (39) and (40) on the basis of a similar Lyapunov analysis (41).

It should be pointed out that some research work on the impedance control employed adaptation rules to deal with uncertain robot dynamics rather than using online impedance variations during HRI. For instance, some neural-networks-based [87], [88], [89], adaptive [90], [91], [92], [93], [94], [95] and nonlinear [96] control strategies have been proposed for HRI applications considering constant impedance elements.

IV. Impedance Learning Methods

Various impedance learning policies have been presented for different HRI tasks in the past decades [45], [61], [97], which can be classified in three categories.

A. Learning from Demonstration (LfD) Approaches

Some LfD methods have been designed as powerful mathematical tools for appropriate adjustment of the robot behavior based on several initial demonstration steps resulting in proper learning for the final execution (imitation) process. This concept has also been broadened to physical HRI and impedance control in recent years. Corresponding LfD-based impedance control studies are described in this section. These methods have been used mostly for learning position trajectories that are similar to those of the human during the demonstration phase, and then for the regulation of robot impedance parameters based on this learning. Thus, they can be utilized in various applications and tasks such as lifting, cutting and physical therapy to achieve optimum path planning, flexibility adjustment and obstacle avoidance [34], [51], [54], [57], [58], [98]. Although LfD-based approaches are model-free, they suffer from lack of stability guarantee in most cases, as expressed in Table I.

1) GMM- and GMR-based Strategies: Gaussian Mixture Models (GMMs) are probabilistic tools that can present a data set via finite numbers of Gaussian distributions. The possibility of modifying Gaussian parameters makes them appropriate for different learning purposes. A two-phase demonstration was employed in [51] to learn both trajectory and impedance of a therapist in a robot-assisted rehabilitation process using a GMM-based strategy. In the first phase, the therapist and patient performed a rehabilitation task simultaneously, and in the second phase, the patient conducted the same task without the therapist's intervention. Their proposed admittance controller [51] generated the desired movement based on the measured force data and the following dynamics

$$\mathbf{f}_e = \mathbf{M}_x^d\ddot{\mathbf{x}}_d + \mathbf{B}_x^d\dot{\mathbf{x}}_d + \mathbf{K}_x^d\mathbf{x}_d \tag{48}$$

where $\mathbf{M}_x^d$, $\mathbf{B}_x^d$, and $\mathbf{K}_x^d$ are the inertia, damping, and stiffness parameters, respectively. The GMMs were expressed as probability density functions in [52] to cluster data gathered from the demonstration phase as

$$P(\mathbf{x}) = \sum_{k=1}^{N_k} p(k)p(\mathbf{x}|k) \tag{49}$$

where $\mathbf{x}$ in [51] denotes the data vector that contains the robot's position, $p(k)$ is the prior, $p(\mathbf{x}|k)$ is the conditional density function and N_k is the number of Gaussian components. The Gaussian parameters $[\pi_k,\ \boldsymbol{\mu}_k,\ \boldsymbol{\Sigma}_k]$ represent the prior probabilities, mean vectors and covariance matrices, respectively, that were calculated using the Expectation Maximum (EM) algorithm. Given these parameters, the activation weight of i^{th} Gaussian function will be obtained as

$$w_i = \frac{\pi_i\mathcal{N}(x|\boldsymbol{\mu}_i, \boldsymbol{\Sigma}_i)}{\sum_{k=1}^{N_k}\pi_k\mathcal{N}(x|\boldsymbol{\mu}_k, \boldsymbol{\Sigma}_k)} \tag{50}$$

The input force to the admittance model (48) was defined as the summation of the environment (E), patient (P) and therapist (T) forces and then simplified as a spring force:

$$\mathbf{f}_e = (\mathbf{K}_E + \mathbf{K}_P + \mathbf{K}_T)(\mathbf{x}_f - \mathbf{x}) \tag{51}$$

where $\mathbf{K}_E$, $\mathbf{K}_P$, and $\mathbf{K}_T$ are the stiffness coefficients of the environment, patient and therapist, and $\mathbf{x}$ is the position of robot end-effector and $\mathbf{x}_f$ is the average of demonstration trajectories. Two combinations of these stiffness values ($\mathbf{K}_E + \mathbf{K}_P + \mathbf{K}_T$ and $\mathbf{K}_E + \mathbf{K}_P$) were investigated from the first and second phases of demonstration, respectively. The spring constant $\mathbf{K}_T$ of the therapist limb could also be calculated as the difference between the two values described above. The Weighted Least Square method (WLS) was employed to estimate the therapist stiffness coefficient associated with each Gaussian component as [51], [53]

$$\mathbf{K}_{T_i}^d = \left[\left(\mathbf{X}^T \mathbf{W}_i \mathbf{X} \right)^{-1} \mathbf{X}^T \mathbf{W}_i \mathbf{F}_T \right] \tag{52}$$

in which $\mathbf{X} = [(\mathbf{x}_f - \mathbf{x}_1), \ldots, (\mathbf{x}_f - \mathbf{x}_N)]^T$, $\mathbf{W}_i = \text{diag}([w_{i_1}, w_{i_2}, ..., w_{i_N}])$, and $\mathbf{F}_T = [\mathbf{f}_{T_1}, \mathbf{f}_{T_2}, ..., \mathbf{f}_{T_N}]$, where N is the number of data samples from all demonstrations. Having the stiffness constants, the approximated therapist force was formulated in the reproduction phase as

$$\mathbf{f}_T = \sum_{i=1}^{N_k} w_i [\mathbf{K}_{T_i}^d (\mathbf{x}_f - \mathbf{x})] \tag{53}$$

A similar approach was developed in [54]; however, the stiffness matrix was estimated by minimizing Euclidean norm of residuals:

$$r_t \left(\mathbf{K}_{x_i}^d \right) = w_i \left(\mathbf{K}_{x_i}^d \tilde{\mathbf{x}}_i - \mathbf{v}(t) \right) \tag{54}$$

where t is the time step, $\mathbf{K}_{x_i}^d$ is the unknown state-dependent stiffness parameter, and $\tilde{\mathbf{x}}_i$ is the deviation with respect to the mean position trajectory corresponds to i^{th} Gaussian function. The right side of this equation represents the designated impedance model in which $\mathbf{v}(t) = \ddot{\mathbf{x}} + \mathbf{B}_x^d \dot{\mathbf{x}} - \mathbf{f}^e$ in which $\mathbf{f}_t^e$ is the measured force signal, and $\mathbf{B}_x^d$ is a preset damping coefficient. Then, a convex optimization problem was formulated in accordance with (54) as follows:

$$\begin{aligned} \min_{\mathbf{K}_{x_i}^d} \quad & \left\| r_t \left(\mathbf{K}_{x_i}^d \right) \right\|_2 \\ \text{s.t.} \quad & \mathbf{K}_{x_i}^d \succeq 0 \end{aligned} \tag{55}$$

Note that interior-point method was adopted in [54] to estimate the stiffness matrix through solving the proposed optimization problem (55). In another study [98], a Bayesian parameter estimation method was adopted to determine the unknown stiffness of the human arm and realize it for the robot as a time-varying element of the impedance model. Similarly, the GMM and EM methods were used to estimate the desired trajectory and the expected force based on the acquired data through demonstrations [55].

The Gaussian Mixture Regression (GMR) was also utilized in [99], [100], [56], [101] to extract the mean trajectory and its covariance ($\boldsymbol{\mu}_i$ and $\boldsymbol{\Sigma}_i$) by GMMs to be implemented in the imitation (reproduction) phase. A Linear Quadratic Regulator (LQR) formulation was defined in [56] to estimate the stiffness and damping matrices via backward integration of the Riccati equation and having a time-varying weighting factor $\mathbf{Q}$ in their cost function for trajectory tracking. A similar GMM-GMR approach was devised in [102], [103] to investigate the average and variability of robot trajectories in rehabilitation and movement therapy tasks. Note that the proposed impedance models in [99], [100], [103] were designed with constant parameters (without having any time-varying change). However, an impedance variation rule was suggested in [102] in terms of the trajectories covariance for physical therapy tasks. The reason behind this variation was mimicking the therapist's interaction stiffness, which is usually selected inversely proportional to the demonstrated variability in order to limit the patient's deviation within the range of demonstrated covariance relative to the mean trajectory [102]. Figure 3 demonstrates the structure of these impedance learning methods in which all GMM-GMR calculations and impedance updating laws can be summarized in the "Impedance Learning Rules" block.

2) DMP-based Strategies: Dynamic Movement Primitives (DMPs) were firstly developed in [104], [105] as a learning tool for autonomous nonlinear dynamical systems. In this regard, EMG signals obtained from able-bodied people have been analyzed in [57], [34], [58] to identify the stiffness (or impedance) and movement of the human limb, and design the robot control objectives based on them. In [34], [58], a DMP-based strategy was presented using nonlinear Gaussian functions formulated for the stiffness regulation as

$$k_x^d(s) = \sum_{i=1}^{N} \gamma_i \phi_i(s) \tag{56}$$

where γ_i is the weighting factor, and $\phi_i(s)$ is the normalized radial basis function having the width of h_i from the center of c_i:

$$\phi_i(s) = \frac{\exp\left(-h_i(s - c_i)^2\right)}{\sum_{j=1}^{N} \exp\left(-h_j(s - c_j)^2\right)} \tag{57}$$

In addition, s in Eqs. (56) and (57) is the state response of a first-order canonical dynamics system defined as

$$\tau \dot{s} = -\alpha_s s \tag{58}$$

in which τ and α_s are constant parameters. In other words, $s \in [0, 1]$ is the phase variable as the normalized version of the time t such that $s(0) = 1$ and $s \to 0$ as $t \to \infty$. This also means that the considered Gaussian function (56) will vanish as $t \to \infty$. In their learning algorithm, the best estimations of weighting factors γ_i were obtained by minimizing the error norm of the human stiffness determined from the measured external force compared with the modeled one by DMPs (56) using an optimized reinforcement learning algorithm.

Another DMP-based method [59] was investigated in which a cost function was designed to minimize the position error, control gains and end-effector acceleration as

$$J = \int_{t_i}^{t_N} 10^3 \text{dis}(x) + 10^{-2} \sum_{j=1}^{n} \left(k_{x_j}^d - k_{x_j}^{d_{min}} \right) + 10^{-3} |\ddot{x}| \, d\rho \tag{59}$$

where $\text{dis}(x)$ is the distance from the robot end-effector to the line path connecting start and end points of movement, k_x^d is the controller's proportional gain, $k_{x_j}^{d_{min}}$ is the minimum stiffness value of j^{th} joint, and $\ddot{x}$ is the end-effector acceleration. In [59], DMPs were taken into account to organize the

trajectory formation, and a reinforcement learning approach was employed to update the parameters of DMPs by minimizing the cost function (59). In other words, updating DMPs coefficients led to the modification of the desired trajectory and the stiffness value.

B. Optimization-based Approaches

Some impedance learning schemes have been investigated based on the optimization of cost functions regarding linear robot impedance and environment/human limb models in the state space. In these studies, the robot dynamics was not taken into account, and optimum coefficients of the desired impedance model have been adjusted via minimizing cost functions (in terms of motion variables and interaction forces), via choosing a human-limb model with known structure but uncertain parameters. Thereby, these impedance-learning strategies were described to be beneficial in various robot interactions with dynamically uncertain environments (human limbs). However, the robot stability was not guaranteed via their corresponding optimal policies in the absence of an analysis of the robot's closed-loop dynamics (as clarified in Table I).

In [60], an unknown time-varying environment (e.g., human limb) was modeled via a second-order differential equation (mass-damper-spring dynamics) as

$$\mathbf{M}_e(t)\ddot{\mathbf{q}}(t) + \mathbf{C}_e(t)\dot{\mathbf{q}}(t) + \mathbf{G}_e(t)\mathbf{q}(t) = \boldsymbol{\tau}_e(t) \tag{60}$$

in which $\mathbf{M}_e(t)$, $\mathbf{C}_e(t)$ and $\mathbf{G}_e(t)$ are unknown time-varying matrices and $\boldsymbol{\tau}_e(t)$ is the HRI torque. For further analyses, Eq. (60) was rewritten in the state space considering $\boldsymbol{\xi}_1(t) = \mathbf{q}(t)$, $\boldsymbol{\xi}_2(t) = \dot{\mathbf{q}}(t)$ and $\boldsymbol{\xi}_3(t) = \int_0^t \boldsymbol{\tau}_e(\sigma)d\sigma$ as three variables:

$$\begin{aligned} \dot{\boldsymbol{\xi}}(t) &= \mathbf{A}(t)\boldsymbol{\xi}(t) + \mathbf{B}(t)\mathbf{u}(t) \\ \mathbf{v}(t) &= \mathbf{C}(t)\boldsymbol{\xi}(t) \end{aligned} \tag{61}$$

where $\mathbf{u}(t) = \boldsymbol{\tau}_e(t)$ and $\mathbf{v}(t)$ are the input and output signals of this system. Based on the Betterment Scheme [60], they proposed a lemma to iteratively update the input as

$$\boldsymbol{\tau}_e^j(t) = \boldsymbol{\tau}_e^{j-1}(t) - \alpha' \left(\dot{\mathbf{v}}^j(t) - \dot{\mathbf{v}}_d(t)\right) \tag{62}$$

in which the parameter α' satisfies $\|\mathbf{I} - \alpha'\mathbf{B}(t)\mathbf{C}(t)\| < 1$. On the other hand, employing a gradient-based scheme for optimizing a cost function $\Gamma(t)$, the following update rules was presented for the interaction torque:

$$\boldsymbol{\tau}_e^j(t) = \boldsymbol{\tau}_e^{j-1}(t) - \beta \left(\frac{\partial \Gamma^j(t)}{\partial \boldsymbol{\tau}_e^j(t)}\right)^T \tag{63}$$

where β is a positive scalar. Then, comparing (62) and (63) resulted in the following relation between the cost function differentiation and the time-derivative of the output variable:

$$\left(\frac{\partial \Gamma^j(t)}{\partial \boldsymbol{\tau}_e^j(t)}\right)^T = \alpha \left(\dot{\mathbf{v}}^j(t) - \dot{\mathbf{v}}_d(t)\right)^T \tag{64}$$

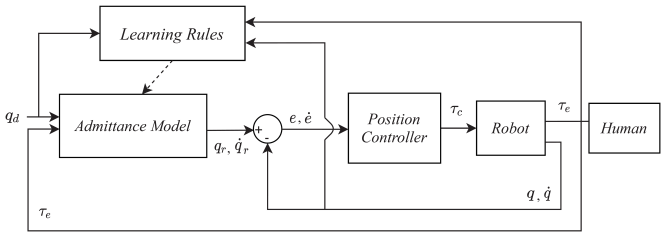

Fig. 3. Schematic diagram of optimization-based learning-based admittance control methods

in which α is defined as α'/β. Moreover, the gradient-based optimization of the cost function $\Gamma(t)$ also led to these adaptation laws for the robot impedance parameters (5):

$$\begin{aligned} \mathbf{B}_x^{d,j}(t) &= \mathbf{B}_x^{d,j-1}(t) - \beta_B \left(\frac{\partial \tau_e^j(t)}{\partial \mathbf{B}_x^{d,j}(t)}\right)^T \left(\frac{\partial \Gamma^j(t)}{\partial \boldsymbol{\tau}_e^j(t)}\right)^T \\ \mathbf{K}_x^{d,j}(t) &= \mathbf{K}_x^{d,j-1}(t) - \beta_K \left(\frac{\partial \tau_e^j(t)}{\partial \mathbf{K}_x^{d,j}(t)}\right)^T \left(\frac{\partial \Gamma^j(t)}{\partial \boldsymbol{\tau}_e^j(t)}\right)^T \end{aligned} \tag{65}$$

where the learning rates β_B and β_K are positive scalars. Substituting (64) into (65) yielded to the final impedance adaptation laws:

$$\begin{aligned} \mathbf{B}_x^{d,j}(t) &= \mathbf{B}_x^{d,j-1}(t) - \alpha\beta_B \dot{\mathbf{e}}^j(t) \left(\dot{\mathbf{v}}^j(t) - \dot{\mathbf{v}}_d(t)\right)^T \\ \mathbf{K}_x^{d,j}(t) &= \mathbf{K}_x^{d,j-1}(t) - \alpha\beta_K \mathbf{e}^j(t) \left(\dot{\mathbf{v}}^j(t) - \dot{\mathbf{v}}_d(t)\right)^T \end{aligned} \tag{66}$$

As seen, the final impedance update rules were obtained in terms of the position and velocity tracking errors ($\mathbf{e}$ and $\dot{\mathbf{e}}$) with an additional multiplier ($\dot{\mathbf{v}}^j - \dot{\mathbf{v}}_d$) based on the specific consideration of the unknown environment dynamics (61). This learning method is schematically depicted in Fig. 3.

An optimal control problem has also been investigated further to obtain effective impedance of the robot and identify the best approximation of the human impedance during HRI. Accordingly, a linear second-order impedance model with an adaptive term was designed for the robot in [61] as

$$\mathbf{M}_q^d\ddot{\mathbf{q}}_m + \mathbf{B}_q^d\dot{\mathbf{q}}_m + \mathbf{K}_q^d q_m = \mathbf{K}_h\mathbf{f}_e + \bar{\mathbf{l}}(q_d) \tag{67}$$

where $\mathbf{M}_q^d$, $\mathbf{B}_q^d$, and $\mathbf{K}_q^d$ are the desired inertia, damping, and stiffness matrices, respectively. Also, $\mathbf{f}_e$ is the human control effort and $\mathbf{K}_h$ is defined as the human force gain in the robot's joint space. The auxiliary input was formulated as $\bar{\mathbf{l}}(q_d) = \mathbf{M}_q^d\mathbf{u}_d + \mathbf{K}_q^d\mathbf{q}_d$. Then, a viscoelastic first-order dynamics was considered for the human arm as

$$\dot{\mathbf{f}}_e = \mathbf{A}_h\mathbf{f}_e + \mathbf{E}_h\bar{\mathbf{e}}_d \tag{68}$$

in which $\mathbf{A}_h$ and $\mathbf{E}_h$ are unknown constants and the position tracking error is defined as $\bar{\mathbf{e}}_d = \bar{\mathbf{q}}_d - \bar{\mathbf{q}}$, where $\bar{\mathbf{q}}_d = \begin{bmatrix}\mathbf{q}_d^T & \dot{\mathbf{q}}_d^T\end{bmatrix}^T$ and $\bar{\mathbf{q}} = \begin{bmatrix}\mathbf{q}_m^T & \dot{\mathbf{q}}_m^T\end{bmatrix}^T$. Having the robot impedance dynamics (5) and presenting it in the error form relative to the reference trajectory, one can write:

$$\begin{aligned} &\dot{\bar{\mathbf{e}}}_d = \mathbf{A}_q\bar{\mathbf{e}}_d + \mathbf{B}_q\mathbf{u}_e, \\ &\mathbf{A}_q = \begin{pmatrix}\mathbf{0} & \mathbf{I} \\ \mathbf{0} & \mathbf{0}\end{pmatrix}, \mathbf{B}_q = \begin{pmatrix}\mathbf{0} \\ \mathbf{I}\end{pmatrix} \\ &\mathbf{u}_e = \left(\mathbf{M}_q^d\right)^{-1}\left(\boldsymbol{\tau}_e + \begin{bmatrix}\mathbf{K}_q^d & \mathbf{B}_q^d\end{bmatrix}\bar{\mathbf{e}}_d\right) \end{aligned} \tag{69}$$

Considering Eqs. (67), (68) and (69), the state-space model of the combined system of the human limb and robot impedance was proposed as follows:

$$\dot{\mathbf{x}} = \underbrace{\begin{pmatrix} \mathbf{A}_q & \mathbf{0} \\ \mathbf{E}_h & \mathbf{A}_h \end{pmatrix}}_{A} \mathbf{x} + \underbrace{\begin{pmatrix} \mathbf{B}_q \\ \mathbf{0} \end{pmatrix}}_{B} \mathbf{u}_e \tag{70}$$

in which $\mathbf{x} = [\bar{\mathbf{e}}_d,\ \mathbf{f}_e]^T$. The performance index was also explained in terms of states and control effort as

$$J = \int_t^{\infty} \left(\mathbf{x}^T \mathbf{Q} \mathbf{x} + \mathbf{u}_e^T \mathbf{R} \mathbf{u}_e\right) \tag{71}$$

where $\mathbf{Q}$ and $\mathbf{R}$ are positive symmetric matrices. The dynamic equation (70) and the performance index (71) were analyzed in an optimal control design by solving an algebraic Riccati equation (ARE) computationally using an integral reinforcement learning (IRL) algorithm. In their iterative policy [61], constant impedance parameters are assumed for the human limb that were estimated over time, and the corresponding robot impedance model was updated as a result of this online estimation.

It is worth mentioning that a similar optimal control problem was adopted in [62] resulted in an ARE solution. Besides, some studies have taken optimal policies for impedance and trajectory adaptation but with model-free reinforcement learning approaches (e.g., the Q-learning method [63]).

C. AI-based Learning Approaches

This section is focused on neural networks (NNs) and fuzzy algorithms for learning the optimum time-varying impedance of the robot for complicated and delicate HRI tasks such as robotic-assisted surgery that needs accurate positioning and velocity control [67], [68]. As highlighted in Table I, to mimic the intelligent decision making process and the physical behavior pattern of human operators, NNs and fuzzy algorithms were utilized to determine and change the robot impedance during the task [64], [65], [66], [67], [68], [69].

A neural network (NN) was designed with multi-layers to adjust the damping element of the robot admittance controller, which was trained to minimize the error between the Cartesian velocity of the robot end-effector and the velocity of minimum jerk trajectory [64]. An NN-based controller with adaptive gains was developed in [65] to realize a prescribed robot impedance, while the impedance model was modified online through a linear quadratic regulator (LQR) technique in order to minimize the human effort. Note that multi-layer neural networks (NNs) have considerable computation costs in some medical and industrial applications with complicated and delicate HRI tasks. Accordingly, fuzzy logic systems have been recently employed by researchers to reduce the state dimension for the kinematics and dynamics analyses of any physical HRI and diminish the computational complexity to achieve rapid training cycles [68].

To this end, the damping coefficient of the robot's admittance controller was regulated in [66], [67] using a Fuzzy Inference System (FIS), having the measurement of the interaction point's velocity and the external force applied by the human operator. The optimum variation of the damping for point-to-point reaching movements was investigated by minimizing the trajectory jerk in two consecutive segments: a rapid motion with low positioning accuracy, and converging to the target with a lower velocity and higher precision [66]. A fuzzy Sarsa (λ)-learning method was developed in [68], [69] for the same purpose of online damping adjustment in a virtual admittance model for robotic-assisted minimally invasive surgery. However, the individual handling behavior of each human operator was learned through a reinforcement strategy to maximize the overall compliance index of the robot. This method was also advanced with a particle-swarm-optimization-based (PSO-based) algorithm to shorten the online training duration [68], [69].

V. Concluding Remarks

A. Current Research Trends

Based on this systematic review of impedance variation and learning for robotic systems during their physical interactions with humans, the following contributions can be delineated.

Linear first- and second-order dynamical systems (including mass, damping and spring elements) have been considered in most studies for the human limb and impedance models due to their simplicity and possibility of implementation in robots, which themselves have second-order nonlinear dynamics. However, more complicated linear impedance models with viscoelastic property and time-varying parameters have also been suggested. This topic is still of paramount importance for formulating and evaluating more realistic human limb and impedance models in HRI applications.

Employing time-varying impedance affects robot stability during physical interactions, although this effect was ignored in some studies. Other studies dealt with stability analyses and investigated allowable levels or appropriate functions, for impedance variation and/or learning, considering the human passivity. In a few other strategies, the robot stability was analyzed in the presence of unstable interactions with the environment (human), while specified dynamic models have been taken into account for the human limb. Accordingly, the stability conditions for implementing time-varying impedance values have been studied with different assumptions, and will remain an active area for future investigations.

Some impedance learning strategies have been augmented by learning the required skills to execute any task. In this regard, appropriate task-specific position trajectories were identified and learned in addition to suitable impedance parameters. In some LfD-based algorithms, a mean trajectory was investigated for the task, and then the impedance variation method was devised based on this trajectory and its covariance. Thus, integrating path planning with impedance adjustment has been explored in recent studies on physical HRI for enhancing robot autonomy in completing tasks via having human-like skill learning.

B. Future Ideas and Challenges

State-of-the-art strategies provide three methodologies for the development of robot impedance skills: optimal and

adaptive control and machine learning. However, due to the restrictions of dynamic modeling in designing model-based controllers and learning from limited kinesthetic signals, more research will be needed to resolve these issues. Areas for future investigation that can advance the progress of impedance learning and variation for HRI applications are presented below.

More realistic but sophisticated dynamic modeling can be developed for the human limb interacting with the robot. For instance, using higher- or fractional-order dynamical systems for the soft human tissue and non-passive human behavior, more advanced time-varying impedance learning/variation will be required. New impedance control strategies with corresponding stability analyses can be explored with more complex and accurate modeling of the human limb.

The challenging trade-off between robot stability and interaction performance still needs to be balanced and requires further investigation. Some studies have focused on improving the human operator's haptic sense and the performance of different HRI tasks. Other research studies were elaborated on manipulating the impedance parameters to guarantee robot stability. Taking these two essential aspects of physical HRI into account simultaneously and achieving a compromise between them would be technically significant.

In some special applications of HRI, including surgery and imaging, the physical interaction of the robot with tissue could be enhanced by image processing and corresponding learning methods. Accordingly, learning algorithms and update rules for robot impedance can be modified and integrated with tissue image analyses. In rehabilitation, movement therapy and other collaborative tasks having social HRI, speech processing and gesture recognition can also be taken into account for impedance adaptation. In these tasks, the human operator can have a variety of choices as the control inputs to the robot in comparison with the current state-of-the-art strategies that employ interaction force and position feedback. With this feature (integrating physical and social HRIs), the robot can comprehend the user's behavior and intention through speech and body language in addition to kinesthetic data. Higher levels of autonomy and new combined learning strategies based on mechanical, visual and vocal data can be areas of future studies.

Impedance learning/variation methods can also be extended for more complex robotic systems. These include tele-robotic systems having two or more leader and follower robots communicating with each other and interacting with human operators and other environments. Further research can address theoretical and technical challenges faced with stability guarantees due to having multiple ports of interaction and impedance models, and the presence of communication delays that potentially increase the instability of a teleoperation system.

ACKNOWLEDGMENT

This work was supported by the Natural Sciences and Engineering Research Council, Canadian Institutes of Health Research, Canada Foundation for Innovation, and the Government of Alberta (Department of Economic Development, Trade and Tourism). VKM is a Canada Research Chair (Tier 1) in Functional Restoration. MS is a recipient of a postdoctoral fellowship award from the SMART Network Innovation Fund.

REFERENCES

[1] M. Sharifi, S. Behzadipour, and G. Vossoughi, "Nonlinear model reference adaptive impedance control for human–robot interactions," *Control Engineering Practice*, vol. 32, pp. 9 – 27, 2014.

[2] A. Bicchi, M. A. Peshkin, and J. E. Colgate, *Safety for Physical Human–Robot Interaction*. Berlin, Heidelberg: Springer Berlin Heidelberg, 2008, pp. 1335–1348.

[3] S. Haddadin and E. Croft, *Physical Human–Robot Interaction*. Cham: Springer International Publishing, 2016, pp. 1835–1874.

[4] N. Hogan, "Impedance Control: An Approach to Manipulation: Part I theory; Part II implementation; Part III applications," *Journal of Dynamic Systems, Measurement, and Control*, vol. 107, no. 1, pp. 1–24, 03 1985.

[5] N. Hogan, "Adaptive control of mechanical impedance by coactivation of antagonist muscles," *IEEE Transactions on Automatic Control*, vol. 29, no. 8, pp. 681–690, 1984.

[6] R. Ikeura, H. Monden, and H. Inooka, "Cooperative motion control of a robot and a human," in *Proceedings of 1994 3rd IEEE International Workshop on Robot and Human Communication*, 1994, pp. 112–117.

[7] M. M. Rahman, R. Ikeura, and K. Mizutani, "Investigating the impedance characteristic of human arm for development of robots to co-operate with human operators," in *IEEE International Conference on Systems, Man, and Cybernetics (SMC)*, vol. 2, 1999, pp. 676–681.

[8] W. S. Newman, "Stability and Performance Limits of Interaction Controllers," *Journal of Dynamic Systems, Measurement, and Control*, vol. 114, no. 4, pp. 563–570, 12 1992.

[9] V. Duchaine, B. Mayer St-Onge, D. Gao, and C. Gosselin, "Stable and intuitive control of an intelligent assist device," *IEEE Transactions on Haptics*, vol. 5, no. 2, pp. 148–159, 2012.

[10] S. P. Buerger and N. Hogan, "Complementary stability and loop shaping for improved human ndash;robot interaction," *IEEE Transactions on Robotics*, vol. 23, no. 2, pp. 232–244, 2007.

[11] K. Lee and M. Buss, "Force tracking impedance control with variable target stiffness," *IFAC Proceedings Volumes*, vol. 41, no. 2, pp. 6751 – 6756, 2008, 17th IFAC World Congress.

[12] D. S. Walker, J. K. Salisbury, and G. Niemeyer, "Demonstrating the benefits of variable impedance to telerobotic task execution," in *IEEE International Conference on Robotics and Automation (ICRA)*, 2011, pp. 1348–1353.

[13] O. Khatib, "A unified approach for motion and force control of robot manipulators: The operational space formulation," *IEEE Journal on Robotics and Automation*, vol. 3, no. 1, pp. 43–53, 1987.

[14] H. P. Huang and S. S. Chen, "Compliant motion control of robots by using variable impedance," *The International Journal of Advanced Manufacturing Technology*, vol. 7, no. 6, pp. 322–332, 1992.

[15] F. Ficuciello, L. Villani, and B. Siciliano, "Variable impedance control of redundant manipulators for intuitive human–robot physical interaction," *IEEE Transactions on Robotics*, vol. 31, no. 4, pp. 850–863, 2015.

[16] R. Ikeura, T. Moriguchi, and K. Mizutani, "Optimal variable impedance control for a robot and its application to lifting an object with a human," in *Proceedings. 11th IEEE International Workshop on Robot and Human Interactive Communication*, 2002, pp. 500–505.

[17] A. Lecours, B. Mayer-St-Onge, and C. Gosselin, "Variable admittance control of a four-degree-of-freedom intelligent assist device," in *IEEE International Conference on Robotics and Automation (ICRA)*, 2012, pp. 3903–3908.

[18] V. Duchaine, B. Mayer St-Onge, D. Gao, and C. Gosselin, "Stable and intuitive control of an intelligent assist device," *IEEE Transactions on Haptics*, vol. 5, no. 2, pp. 148–159, 2012.

[19] V. Duchaine and C. M. Gosselin, "General model of human-robot cooperation using a novel velocity based variable impedance control," in *Second Joint EuroHaptics Conference and Symposium on Haptic Interfaces for Virtual Environment and Teleoperator Systems (WHC'07)*, 2007, pp. 446–451.

[20] R. V. Dubey, Tan Fung Chan, and S. E. Everett, "Variable damping impedance control of a bilateral telerobotic system," *IEEE Control Systems Magazine*, vol. 17, no. 1, pp. 37–45, 1997.

[21] C. Mitsantisuk, K. Ohishi, and S. Katsura, "Variable mechanical stiffness control based on human stiffness estimation," in *IEEE International Conference on Mechatronics*, 2011, pp. 731–736.

[22] M. S. Erden and A. Billard, "Robotic assistance by impedance compensation for hand movements while manual welding," *IEEE transactions on cybernetics*, vol. 46, no. 11, pp. 2459–2472, 2015.

[23] M. S. Erden and B. Marić, "Assisting manual welding with robot," *Robotics and Computer-Integrated Manufacturing*, vol. 27, no. 4, pp. 818–828, 2011.

[24] R. Ikeura and H. Inooka, "Variable impedance control of a robot for cooperation with a human," in *IEEE International Conference on Robotics and Automation (ICRA)*, vol. 3, 1995, pp. 3097–3102.

[25] T. Tsumugiwa, R. Yokogawa, and K. Hara, "Variable impedance control with regard to working process for man-machine cooperation-work system," in *IEEE/RSJ International Conference on Intelligent Robots and Systems (IROS). Expanding the Societal Role of Robotics in the the Next Millennium*, vol. 3, 2001, pp. 1564–1569.

[26] T. Tsumugiwa, R. Yokogawa, and K. Hara, "Variable impedance control based on estimation of human arm stiffness for human-robot cooperative calligraphic task," in *IEEE International Conference on Robotics and Automation (ICRA)*, vol. 1, 2002, pp. 644–650.

[27] T. Tsumugiwa, R. Yokogawa, and K. Hara, "Variable impedance control with virtual stiffness for human-robot cooperative peg-in-hole task," in *IEEE/RSJ International Conference on Intelligent Robots and Systems (IROS)*, vol. 2, 2002, pp. 1075–1081.

[28] A. Taherifar, G. Vossoughi, and A. Selk Ghafari, "Optimal target impedance selection of the robot interacting with human," *Advanced Robotics*, vol. 31, no. 8, pp. 428–440, 2017.

[29] F. Müller, J. Janetzky, U. Behrnd, J. Jäkel, and U. Thomas, "User force-dependent variable impedance control in human-robot interaction," in *IEEE 14th International Conference on Automation Science and Engineering (CASE)*, 2018, pp. 1328–1335.

[30] A. Ajoudani, N. Tsagarakis, and A. Bicchi, "Tele-impedance: Teleoperation with impedance regulation using a body–machine interface," *The International Journal of Robotics Research*, vol. 31, no. 13, pp. 1642–1656, 2012.

[31] L. Masia and V. Squeri, "A modular mechatronic device for arm stiffness estimation in human–robot interaction," *IEEE/ASME Transactions on Mechatronics*, vol. 20, no. 5, pp. 2053–2066, 2014.

[32] W. Gallagher, D. Gao, and J. Ueda, "Improved stability of haptic human–robot interfaces using measurement of human arm stiffness," *Advanced Robotics*, vol. 28, no. 13, pp. 869–882, 2014.

[33] Y.-J. Kim, C.-K. Park, and K. G. Kim, "An emg-based variable impedance control for elbow exercise: preliminary study," *Advanced Robotics*, vol. 31, no. 15, pp. 809–820, 2017.

[34] C. Yang, C. Zeng, C. Fang, W. He, and Z. Li, "A dmps-based framework for robot learning and generalization of humanlike variable impedance skills," *IEEE/ASME Transactions on Mechatronics*, vol. 23, no. 3, pp. 1193–1203, 2018.

[35] A. Ajoudani, C. Fang, N. Tsagarakis, and A. Bicchi, "Reduced-complexity representation of the human arm active endpoint stiffness for supervisory control of remote manipulation," *The International Journal of Robotics Research*, vol. 37, no. 1, pp. 155–167, 2018.

[36] S. Grafakos, F. Dimeas, and N. Aspragathos, "Variable admittance control in phri using emg-based arm muscles co-activation," in *IEEE International Conference on Systems, Man, and Cybernetics (SMC)*, 2016, pp. 1900–1905.

[37] C. Ott, *Cartesian impedance control of redundant and flexible-joint robots*. Springer, 2008.

[38] F. Ferraguti, C. Secchi, and C. Fantuzzi, "A tank-based approach to impedance control with variable stiffness," in *IEEE International Conference on Robotics and Automation (ICRA)*, 2013, pp. 4948–4953.

[39] C. Schindlbeck and S. Haddadin, "Unified passivity-based cartesian force/impedance control for rigid and flexible joint robots via task-energy tanks," in *IEEE International Conference on Robotics and Automation (ICRA)*, 2015, pp. 440–447.

[40] F. Ferraguti, N. Preda, A. Manurung, M. Bonfè, O. Lambercy, R. Gassert, R. Muradore, P. Fiorini, and C. Secchi, "An energy tank-based interactive control architecture for autonomous and teleoperated robotic surgery," *IEEE Transactions on Robotics*, vol. 31, no. 5, pp. 1073–1088, 2015.

[41] K. Kronander and A. Billard, "Stability considerations for variable impedance control," *IEEE Transactions on Robotics*, vol. 32, no. 5, pp. 1298–1305, 2016.

[42] Y. Dong and B. Ren, "UDE-based variable impedance control of uncertain robot systems," *IEEE Transactions on Systems, Man, and Cybernetics: Systems*, 2017.

[43] C. Secchi and F. Ferraguti, "Energy optimization for a robust and flexible interaction control," in *International Conference on Robotics and Automation (ICRA)*, 2019, pp. 1919–1925.

[44] T. Sun, L. Peng, L. Cheng, Z. Hou, and Y. Pan, "Stability-guaranteed variable impedance control of robots based on approximate dynamic inversion," *IEEE Transactions on Systems, Man, and Cybernetics: Systems*, vol. 0, no. 0, pp. 1–8, 2019.

[45] C. Yang, G. Ganesh, S. Haddadin, S. Parusel, A. Albu-Schaeffer, and E. Burdet, "Human-like adaptation of force and impedance in stable and unstable interactions," *IEEE Transactions on Robotics*, vol. 27, no. 5, pp. 918–930, 2011.

[46] G. Ganesh, A. Albu-Schäffer, M. Haruno, M. Kawato, and E. Burdet, "Biomimetic motor behavior for simultaneous adaptation of force, impedance and trajectory in interaction tasks," in *IEEE International Conference on Robotics and Automation (ICRA)*, 2010, pp. 2705–2711.

[47] E. Burdet, G. Ganesh, C. Yang, and A. Albu-Schäffer, *Interaction Force, Impedance and Trajectory Adaptation: By Humans, for Robots*. Berlin, Heidelberg: Springer Berlin Heidelberg, 2014, pp. 331–345.

[48] P. Liang, C. Yang, N. Wang, Z. Li, R. Li, and E. Burdet, "Implementation and test of human-operated and human-like adaptive impedance controls on baxter robot," in *Advances in Autonomous Robotics Systems*, M. Mistry, A. Leonardis, M. Witkowski, and C. Melhuish, Eds. Cham: Springer International Publishing, 2014, pp. 109–119.

[49] Y. Li, G. Ganesh, N. Jarrassé, S. Haddadin, A. Albu-Schaeffer, and E. Burdet, "Force, impedance, and trajectory learning for contact tooling and haptic identification," *IEEE Transactions on Robotics*, vol. 34, no. 5, pp. 1170–1182, 2018.

[50] Y. Li, X. Zhou, J. Zhong, and X. Li, "Robotic impedance learning for robot-assisted physical training," *Frontiers in Robotics and AI*, vol. 6, p. 78, 2019.

[51] J. Fong and M. Tavakoli, "Kinesthetic teaching of a therapist's behavior to a rehabilitation robot," in *2018 International Symposium on Medical Robotics (ISMR)*, 2018, pp. 1–6.

[52] S. Calinon, *Robot programming by demonstration*. EPFL Press, 2009.

[53] L. D. Rozo, S. Calinon, D. Caldwell, P. Jiménez, and C. Torras, "Learning collaborative impedance-based robot behaviors," in *Twenty-Seventh AAAI Conference on Artificial Intelligence*, 2013.

[54] L. Rozo, S. Calinon, D. G. Caldwell, P. Jimenez, and C. Torras, "Learning physical collaborative robot behaviors from human demonstrations," *IEEE Transactions on Robotics*, vol. 32, no. 3, pp. 513–527, 2016.

[55] E. Gribovskaya, A. Kheddar, and A. Billard, "Motion learning and adaptive impedance for robot control during physical interaction with humans," in *IEEE International Conference on Robotics and Automation (ICRA)*, 2011, pp. 4326–4332.

[56] S. Calinon, D. Bruno, and D. G. Caldwell, "A task-parameterized probabilistic model with minimal intervention control," in *IEEE International Conference on Robotics and Automation (ICRA)*, 2014, pp. 3339–3344.

[57] C. Yang, C. Zeng, P. Liang, Z. Li, R. Li, and C. Su, "Interface design of a physical human–robot interaction system for human impedance adaptive skill transfer," *IEEE Transactions on Automation Science and Engineering*, vol. 15, no. 1, pp. 329–340, 2018.

[58] C. Yang, C. Zeng, Y. Cong, N. Wang, and M. Wang, "A learning framework of adaptive manipulative skills from human to robot," *IEEE Transactions on Industrial Informatics*, vol. 15, no. 2, pp. 1153–1161, 2019.

[59] F. Stulp, J. Buchli, A. Ellmer, M. Mistry, E. A. Theodorou, and S. Schaal, "Model-free reinforcement learning of impedance control in stochastic environments," *IEEE Transactions on Autonomous Mental Development*, vol. 4, no. 4, pp. 330–341, 2012.

[60] Y. Li and S. S. Ge, "Impedance learning for robots interacting with unknown environments," *IEEE Transactions on Control Systems Technology*, vol. 22, no. 4, pp. 1422–1432, 2014.

[61] Z. Li, J. Liu, Z. Huang, Y. Peng, H. Pu, and L. Ding, "Adaptive impedance control of human–robot cooperation using reinforcement learning," *IEEE Transactions on Industrial Electronics*, vol. 64, no. 10, pp. 8013–8022, 2017.

[62] S. S. Ge, Y. Li, and C. Wang, "Impedance adaptation for optimal robot–environment interaction," *International Journal of Control*, vol. 87, no. 2, pp. 249–263, 2014.

[63] R. Yang, C. Yang, M. Chen, and J. Na, "Adaptive impedance control of robot manipulators based on q-learning and disturbance observer," *Systems Science & Control Engineering*, vol. 5, no. 1, pp. 287–300, 2017.

[64] A. Sharkawy, P. N. Koustournpardis, and N. Aspragathos, "Variable admittance control for human-robot collaboration based on online neural network training," in *IEEE/RSJ International Conference on Intelligent Robots and Systems (IROS)*, 2018, pp. 1334–1339.

[65] H. Modares, I. Ranatunga, F. L. Lewis, and D. O. Popa, "Optimized assistive human–robot interaction using reinforcement learning," *IEEE Transactions on Cybernetics*, vol. 46, no. 3, pp. 655–667, 2016.

[66] F. Dimeas and N. Aspragathos, "Fuzzy learning variable admittance control for human-robot cooperation," in *IEEE/RSJ International Conference on Intelligent Robots and Systems (IROS)*, 2014, pp. 4770–4775.

[67] S. Kuang, Y. Tang, A. Lin, S. Yu, and L. Sun, *Intelligent Control for Human-Robot Cooperation in Orthopedics Surgery*. Singapore: Springer Singapore, 2018, pp. 245–262.

[68] W. Wang, C. Du, W. Wang, and Z. Du, "A pso-optimized fuzzy reinforcement learning method for making the minimally invasive surgical arm cleverer," *IEEE Access*, vol. 7, pp. 48 655–48 670, 2019.

[69] Z. Du, W. Wang, Z. Yan, W. Dong, and W. Wang, "Variable admittance control based on fuzzy reinforcement learning for minimally invasive surgery manipulator," *Sensors*, vol. 17, no. 4, p. 844 (15 pages), 2017.

[70] X. Xiaohu, Z. Dahu, H. Zhang, Y. Sijie, and D. Han, "Application of novel force control strategies to enhance robotic abrasive belt grinding quality of aero-engine blades," *Chinese Journal of Aeronautics*, vol. 32, no. 10, pp. 2368–2382, 2019.

[71] L. Roveda, N. Pedrocchi, M. Beschi, and L. M. Tosatti, "High-accuracy robotized industrial assembly task control schema with force overshoots avoidance," *Control Engineering Practice*, vol. 71, pp. 142–153, 2018.

[72] H. Kazerooni, "Automated robotic deburring using impedance control," *IEEE Control Systems Magazine*, vol. 8, no. 1, pp. 21–25, 1988.

[73] L. Cheng and M. Tavakoli, "Ultrasound image guidance and robot impedance control for beating-heart surgery," *Control Engineering Practice*, vol. 81, pp. 9–17, 2018.

[74] D. Surdilovic and Z. Cojbasic, "Robust robot compliant motion control using intelligent adaptive impedance approach," in *IEEE International Conference on Robotics and Automation (ICRA)*, vol. 3, 1999, pp. 2128–2133.

[75] L. Bi, C. Guan *et al.*, "A review on emg-based motor intention prediction of continuous human upper limb motion for human-robot collaboration," *Biomedical Signal Processing and Control*, vol. 51, pp. 113–127, 2019.

[76] A. Albu-Schäffer, C. Ott, and G. Hirzinger, "A unified passivity-based control framework for position, torque and impedance control of flexible joint robots," *The international journal of robotics research*, vol. 26, no. 1, pp. 23–39, 2007.

[77] A. Albu-Schäffer, S. Haddadin, C. Ott, A. Stemmer, T. Wimböck, and G. Hirzinger, "The dlr lightweight robot: design and control concepts for robots in human environments," *Industrial Robot: an international journal*, vol. 34, no. 5, pp. 376–385, 2007.

[78] C. Rossa, N. Usmani, R. Sloboda, and M. Tavakoli, "A hand-held assistant for semiautomated percutaneous needle steering," *IEEE Transactions on Biomedical Engineering*, vol. 64, no. 3, pp. 637–648, 2016.

[79] M. Khadem, C. Rossa, N. Usmani, R. S. Sloboda, and M. Tavakoli, "Robotic-assisted needle steering around anatomical obstacles using notched steerable needles," *IEEE Journal of Biomedical and Health Informatics*, vol. 22, no. 6, pp. 1917–1928, 2017.

[80] M. Sharifi, H. Salarieh, S. Behzadipour, and M. Tavakoli, "Beating-heart robotic surgery using bilateral impedance control: Theory and experiments," *Biomedical signal processing and control*, vol. 45, pp. 256–266, 2018.

[81] L. Barbé, B. Bayle, M. De Mathelin, and A. Gangi, "Online robust model estimation and haptic clues detection during in vivo needle insertions," in *IEEE International Conference on Biomedical Robotics and Biomechatronics (BioRob)*, 2006, pp. 341–346.

[82] D. Lee and K. Huang, "Passive-set-position-modulation framework for interactive robotic systems," *IEEE Transactions on Robotics*, vol. 26, no. 2, pp. 354–369, 2010.

[83] B. Zhou, "On asymptotic stability of linear time-varying systems," *Automatica*, vol. 68, pp. 266–276, 2016.

[84] Q. C. Zhong and D. Rees, "Control of uncertain lti systems based on an uncertainty and disturbance estimator," *Journal of dynamic systems, measurement, and control*, vol. 126, no. 4, pp. 905–910, 2004.

[85] K. P. Tee, D. W. Franklin, M. Kawato, T. E. Milner, and E. Burdet, "Concurrent adaptation of force and impedance in the redundant muscle system," *Biological Cybernetics*, vol. 102, no. 1, pp. 31–44, Jan 2010.

[86] C. Yang and E. Burdet, "A model of reference trajectory adaptation for interaction with objects of arbitrary shape and impedance," in *IEEE/RSJ International Conference on Intelligent Robots and Systems (IROS)*, 2011, pp. 4121–4126.

[87] Y. Li, S. S. Ge, Q. Zhang, and T. H. Lee, "Neural networks impedance control of robots interacting with environments," *IET Control Theory Applications*, vol. 7, no. 11, pp. 1509–1519, 2013.

[88] H. Huang, C. Yang, Z. Ju, Y. Yuan, and Z. Li, "Broad fuzzy neural control using impedance learning," in *IEEE 4th International Conference on Advanced Robotics and Mechatronics (ICARM)*, 2019, pp. 173–178.

[89] C. Yang, G. Peng, Y. Li, R. Cui, L. Cheng, and Z. Li, "Neural networks enhanced adaptive admittance control of optimized robot–environment interaction," *IEEE Transactions on Cybernetics*, vol. 49, no. 7, pp. 2568–2579, 2019.

[90] Y. Li, S. Sam Ge, and C. Yang, "Learning impedance control for physical robot–environment interaction," *International Journal of Control*, vol. 85, no. 2, pp. 182–193, 2012.

[91] M. Sharifi, S. Behzadipour, and G. Vossoughi, "Model reference adaptive impedance control in cartesian coordinates for physical human–robot interaction," *Advanced Robotics*, vol. 28, no. 19, pp. 1277–1290, 2014.

[92] L. Kong, W. He, C. Yang, Z. Li, and C. Sun, "Adaptive fuzzy control for coordinated multiple robots with constraint using impedance learning," *IEEE Transactions on Cybernetics*, vol. 49, no. 8, pp. 3052–3063, 2019.

[93] M. Sharifi, S. Behzadipour, and H. Salarieh, "Nonlinear Bilateral Adaptive Impedance Control With Applications in Telesurgery and Telerehabilitation," *Journal of Dynamic Systems, Measurement, and Control*, vol. 138, no. 11, 07 2016, 111010.

[94] T. Sun, L. Peng, L. Cheng, Z. Hou, and Y. Pan, "Composite learning enhanced robot impedance control," *IEEE Transactions on Neural Networks and Learning Systems*, vol. 0, no. 0, pp. 1–8, 2019.

[95] M. Sharifi, H. Salarieh, S. Behzadipour, and M. Tavakoli, "Tele-echography of moving organs using an impedance-controlled telerobotic system," *Mechatronics*, vol. 45, pp. 60 – 70, 2017.

[96] Y. Jiang, C. Yang, Z. Ju, A. Annamalai, and H. Liu, "Compliant impedance control for a redundant manipulator during human robot interaction," in *24th International Conference on Automation and Computing (ICAC)*, 2018, pp. 1–6.

[97] G. Ganesh, N. Jarrassé, S. Haddadin, A. Albu-Schaeffer, and E. Burdet, "A versatile biomimetic controller for contact tooling and haptic exploration," in *IEEE International Conference on Robotics and Automation (ICRA)*, 2012, pp. 3329–3334.

[98] X. Yu, W. He, Y. Li, C. Xue, J. Li, J. Zou, and C. Yang, "Bayesian estimation of human impedance and motion intention for human-robot collaboration," *IEEE Transactions on Cybernetics*, pp. 1–13, 2019.

[99] J. Fong, C. Martinez, and M. Tavakoli, "Ways to learn a therapist's patient-specific intervention: Robotics vs telerobotics-mediated hands-on teaching," in *International Conference on Robotics and Automation (ICRA)*, 2019, pp. 870–876.

[100] J. Fong, H. Rouhani, and M. Tavakoli, "A therapist-taught robotic system for assistance during gait therapy targeting foot drop," *IEEE Robotics and Automation Letters*, vol. 4, no. 2, pp. 407–413, 2019.

[101] L. Rozo, S. Calinon, and D. G. Caldwell, "Learning force and position constraints in human-robot cooperative transportation," in *The 23rd IEEE International Symposium on Robot and Human Interactive Communication*, 2014, pp. 619–624.

[102] M. Najafi, K. Adams, and M. Tavakoli, "Robotic learning from demonstration of therapist's time-varying assistance to a patient in trajectory-following tasks," in *International Conference on Rehabilitation Robotics (ICORR)*, 2017, pp. 888–894.

[103] M. Najafi, M. Sharifi, K. Adams, and M. Tavakoli, "Robotic assistance for children with cerebral palsy based on learning from tele-cooperative demonstration," *International Journal of Intelligent Robotics and Applications*, vol. 1, no. 1, pp. 43–54, Feb 2017.

[104] S. Schaal, P. Mohajerian, and A. Ijspeert, "Dynamics systems vs. optimal control—a unifying view," *Progress in brain research*, vol. 165, pp. 425–445, 2007.

[105] A. J. Ijspeert, J. Nakanishi, H. Hoffmann, P. Pastor, and S. Schaal, "Dynamical movement primitives: Learning attractor models for motor behaviors," *Neural Computation*, vol. 25, no. 2, pp. 328–373, 2013.

Mojtaba Sharifi is a postdoctoral research fellow in the Department of Electrical and Computer Engineering and the Department of Medicine, University of Alberta, Canada. He received his B.Sc. and M.Sc. degrees in Mechanical Engineering from Shiraz University and Sharif University of Technology, Iran, in 2010 and 2012, respectively. He conducted a collaborative research project in the Telerobotic and Biorobotic Systems Lab of the University of Alberta, Canada, from 2015 to 2016, and earned his Ph.D. degree from Sharif University of Technology, Iran, in 2017. His interdisciplinary research includes control, dynamics and design of robots (in biomedical applications: rehabilitation, surgery and imaging), human-robot interaction (using impedance control and learning), haptics, collaborative robotics and tele-robotics (using bilateral and multilateral control), wearable and assistive robotics (exoskeleton, prosthesis and orthosis), control and modeling of musculoskeletal systems, and biological systems.

Amir Zakerimanesh received his B.Sc. and M.Sc. degrees in electrical engineering (control-system) both from the Faculty of Electrical and Computer Engineering, University of Tabriz, Tabriz, Iran, in 2012 and 2015, respectively. He is currently pursuing a Ph.D. in Electrical Engineering at the University of Alberta. His research interests include machine learning, intelligent transportation systems, teleoperation systems, and control engineering.

Javad K. Mehr received his B.Sc. and M.Sc. degrees in Mechanical Engineering from the University of Tabriz in 2015 and Shiraz University in 2019. He is currently pursuing a Ph.D. degree in the Department of Electrical and Computer Engineering and the Department of Medicine at the University of Alberta. His research interests are modeling and controlling robotic systems in medical applications with a focus on lower-limb rehabilitation.

Ali Torabi is a postdoctoral fellow at the University of Alberta. He received the BSc degree in mechanical engineering from Amirkabir University of Technology (Tehran Polytechnic) in 2010 and the MSc degree in mechanical engineering from Sharif University of Technology in 2013. He received his PhD degree in Electrical and Computer Engineering from the University of Alberta in 2020. In 2014-2016, he was a researcher at Research Center for Intelligent Neuro Rehabilitation Technology, Iran. His research interests include medical robotics, control engineering, and teleoperation systems.

Vivian K. Mushahwar received her B.Sc. degree in electrical engineering from Brigham Young University, Provo, UT, USA in 1991 and a Ph.D. degree in bioengineering from the University of Utah, Salt Lake City, USA in 1996. She received postdoctoral training at Emory University, Atlanta, GA, USA and the University of Alberta, Edmonton, AB, Canada. She is currently a professor in the Department of Medicine, Division of Physical Medicine and Rehabilitation at the University of Alberta, a Canada Research Chair (Tier 1) in Functional Restoration, and a Killam Professor. She is also the director of the Sensory Motor Adaptive Rehabilitation Technology (SMART) Network at the University of Alberta. Her research interests include identification of spinal-cord systems involved in locomotion, development of spinal-cord-based neural prostheses for restoring mobility after spinal cord injury, identification of rehabilitation interventions for enhancing mobility, and the use of active intelligent wearable devices for preventing secondary complications associated with neurological conditions including spasticity, pressure injuries, and deep vein thrombosis.

Mahdi Tavakoli is a Professor in the Department of Electrical and Computer Engineering, University of Alberta, Canada. He received his BSc and MSc degrees in Electrical Engineering from Ferdowsi University and K.N. Toosi University, Iran, in 1996 and 1999, respectively. He received his PhD degree in Electrical and Computer Engineering from the University of Western Ontario, Canada, in 2005. In 2006, he was a post-doctoral researcher at Canadian Surgical Technologies and Advanced Robotics (CSTAR), Canada. In 2007-2008, he was an NSERC Post-Doctoral Fellow at Harvard University, USA. Dr. Tavakoli's research interests broadly involve the areas of robotics and systems control. Specifically, his research focuses on haptics and teleoperation control, medical robotics, and image-guided surgery. Dr. Tavakoli is the lead author of Haptics for Teleoperated Surgical Robotic Systems (World Scientific, 2008). He is a Senior Member of IEEE and an Associate Editor for IEEE/ASME Transactions on Mechatronics, Journal of Medical Robotics Research, Control Engineering Practice, and Mechatronics.